

## SCIENCE OF TSUNAMI HAZARDS

Journal of Tsunami Society International

Volume 32

Number 1

2013

### THE FRENCH TSUNAMI WARNING CENTER FOR THE MEDITERRANEAN AND NORTHEAST ATLANTIC: CENALT

1

**P. Roudil, F. Schindel , R. Bossu, N. Alabrune, P. Arnoul, P. Duperray, A. Gailler, J. Guilbert, H. H bert, and A. Loevenbruck**

*Commissariat   l' nergie atomique et aux  nergies alternatives alternatives (CEA), CEA/DIF/DASE  
Bruy res-le-Ch tel, FRANCE*

### SEVERAL TSUNAMI SCENARIOS AT THE NORTH SEA AND THEIR CONSEQUENCES AT THE GERMAN BIGHT

8

**Silvia Chac n-Barrantes** - *Departamento de F sica, Universidad Nacional de Costa Rica, Heredia, COSTA RICA, Now at the Coastal Research Laboratory, University of Kiel, GERMANY*

**Rangaswami Narayanan** - *Formerly, Reader, Department of Civil and Structural Engineering, University of Manchester, Manchester, UNITED KINGDOM*

**Roberto Mayerle** - *Coastal Research Laboratory, University of Kiel, GERMANY*

### ASSESSMENT OF TSUNAMI GENERATION POTENTIAL THROUGH RAPID ANALYSIS OF SEISMIC PARAMETERS - Case study: Comparison of the Sumatra Earthquakes of 6 April and 25 October 2010

29

**Madlazim** - *Physics Department, Faculty of Mathematics and Sciences, Surabaya State University (UNESA) Jl. Ketintang, Surabaya 60231, INDONESIA*

### USING FOURIER TRANSFORM INFRARED (FTIR) TO CHARACTERIZE TSUNAMI DEPOSITS IN NEAR-SHORE AND COASTAL WATERS OF THAILAND

**S. Pongpiachan<sup>1\*</sup>, K. Thumanu<sup>2</sup>, W. Na Phatthalung<sup>2</sup>, D. Tipmanee<sup>3,4</sup>, P. Kanchai<sup>1</sup>, P. Feldens<sup>5</sup> and K. Schwarzer<sup>6</sup>**

39

<sup>1</sup>*NIDA Center for Research & Development of Disaster Prevention & Management, School of Social and Environmental Development, National Institute of Development Administration (NIDA), Bangkok, THAILAND*

<sup>2</sup>*Synchrotron Light Research Institute (Public Organization), Ministry of Science and Technology, THAILAND*

<sup>3</sup>*International Postgraduate Program in Environmental Management, Graduate School, Chulalongkorn University, Bangkok, THAILAND*

<sup>4</sup>*Center of Excellence for Environmental and Hazardous Waste Management (EHWM), Chulalongkorn University, Bangkok, THAILAND*

<sup>5</sup>*GEOMAR Helmholtz Centre for Ocean Research Kiel, GERMANY*

<sup>6</sup>*Institute of Geosciences Sedimentology, Coastal and Continental Shelf Research, Christian Albrechts University of Kiel, Kiel, GERMANY*

*TSUNAMI SOCIETY INTERNATIONAL, 1741 Ala Moana Blvd. #70, Honolulu, HI 96815, USA.*

*SCIENCE OF TSUNAMI HAZARDS is a CERTIFIED OPEN ACCESS Journal included in the prestigious international academic journal database DOAJ, maintained by the University of Lund in Sweden with the support of the European Union. SCIENCE OF TSUNAMI HAZARDS is also preserved, archived and disseminated by the National Library, The Hague, NETHERLANDS, the Library of Congress, Washington D.C., USA, the Electronic Library of Los Alamos, National Laboratory, New Mexico, USA, the EBSCO Publishing databases and ELSEVIER Publishing in Amsterdam. The vast dissemination gives the journal additional global exposure and readership in 90% of the academic institutions worldwide, including nation-wide access to databases in more than 70 countries.*

**OBJECTIVE:** Tsunami Society International publishes this interdisciplinary journal to increase and disseminate knowledge about tsunamis and their hazards.

**DISCLAIMER:** Although the articles in SCIENCE OF TSUNAMI HAZARDS have been technically reviewed by peers, Tsunami Society International is not responsible for the veracity of any statement, opinion or consequences.

#### **EDITORIAL STAFF**

Dr. George Pararas-Carayannis, Editor  
<mailto:drgeorgepc@yahoo.com>

#### **EDITORIAL BOARD**

Dr. Charles MADER, Mader Consulting Co., Colorado, New Mexico, Hawaii, USA  
Dr. Hermann FRITZ, Georgia Institute of Technology, USA  
Prof. George CURTIS, University of Hawaii -Hilo, USA  
Dr. Tad S. MURTY, University of Ottawa, CANADA  
Dr. Zygmunt KOWALIK, University of Alaska, USA  
Dr. Galen GISLER, NORWAY  
Prof. Kam Tim CHAU, Hong Kong Polytechnic University, HONG KONG  
Dr. Jochen BUNDSCHUH, (ICE) COSTA RICA, Royal Institute of Technology, SWEDEN  
Dr. Yurii SHOKIN, Novosibirsk, RUSSIAN FEDERATION

#### **TSUNAMI SOCIETY INTERNATIONAL, OFFICERS**

Dr. George Pararas-Carayannis, President;  
Dr. Tad Murty, Vice President;  
Dr. Carolyn Forbes, Secretary/Treasurer.

Submit manuscripts of research papers, notes or letters to the Editor. If a research paper is accepted for publication the author(s) must submit a scan-ready manuscript, a Doc, TeX or a PDF file in the journal format. Issues of the journal are published electronically in PDF format. There is a minimal publication fee for authors who are members of Tsunami Society International for three years and slightly higher for non-members. Tsunami Society International members are notified by e-mail when a new issue is available. Permission to use figures, tables and brief excerpts from this journal in scientific and educational works is granted provided that the source is acknowledged.

Recent and all past journal issues are available at: <http://www.TsunamiSociety.org> CD-ROMs of past volumes may be purchased by contacting Tsunami Society International at [postmaster@tsunamisociety.org](mailto:postmaster@tsunamisociety.org) Issues of the journal from 1982 thru 2005 are also available in PDF format at the Los Alamos National Laboratory Library <http://epubs.lanl.gov/tsunami/>



**THE FRENCH TSUNAMI WARNING CENTER FOR THE MEDITERRANEAN AND  
NORTHEAST ATLANTIC: CENALT**

**P. Roudil, F. Schindel , R. Bossu, N. Alabrune, P. Arnoul, P. Duperray, A. Gailler, J. Guilbert,**

**H. H bert, A. Loevenbruck**

*Commissariat   l' nergie atomique et aux  nergies alternatives  
CEA/DIF/DASE  
Bruy res-le-Ch tel  
FRANCE*

**ABSTRACT**

CENALT (CENTre d'ALerte aux Tsunamis) is responsible for the French National Tsunami Warning Centre (NTWC). The CENALT is established in the framework of the Unesco/IOC/ICG/NEAMTWS. Its objective is to transmit a warning message in less than fifteen minutes for any events that could trigger a tsunami in the Western Mediterranean Sea and the North-Eastern Atlantic Ocean. The data collected from French installations and from institutions of European and North African countries is processed with software that permits early epicenter location of seismic events and measurements of expected tsunami impacts on the shore. On-duty analysts revise interactively all the generated information and use references of historical tsunami and earthquake databases - as well as computed tsunami scenarios - in order to disseminate the more comprehensive message possible.

**Keywords:** *Tsunami, warning, centre, France, Mediterranean, Atlantic*

## **1. CREATION OF THE CENALT PROJECT**

Following the first international meeting on tsunami alert systems in the Mediterranean in November 2005, the French interior ministry on April 2006 tasked the Commissariat à l'énergie atomique et aux énergies alternatives (CEA) to implement a tsunami warning system in the Mediterranean. In November 2007, France officially announced its intention to host a tsunami-warning centre for the Western Mediterranean. On 22 September 2009, an agreement was signed, linking the two Ministries of Interior and Sustainable Development with the CEA, the French Hydrographic and Oceanographic Service (SHOM) and the Centre National de la Recherche Scientifique (CNRS), for the purpose of developing and operating the warning system and the centre. The CEA proposal included the establishment of dedicated stations of institutions around the Western Mediterranean to obtain seismic data that was important in detecting and measuring seismic events. Contacts were made and several stations were established with institutions from different countries as well as the CTBTO, thanks to the agreement signed in 2008 between CTBTO and Unesco. The collaboration with these institutions is presently working well and there has been good response since the agreed transmission of data begun. In accordance with the initially scheduled proposal, the CENALT entered into operation on the 1<sup>st</sup> of July 2012.

## **2. CENALT OPERATIONS**

The objective of CENALT is to monitor the Western Mediterranean Sea and the North-Eastern Atlantic region for seismic events that could trigger tsunamis. Due to the proximity of seismic sources to monitored coastlines, the Centre is tasked with the responsibility of sending the first message to the French civil protection and to the Member states of the NEAM region within a window of time of less than fifteen minutes. To be able to comply with this short-term goal, it became necessary to establish permanent, technical analyst presence at the Centre in order to monitor effectively data reception and to process and disseminate advisory/warning information.

### **2.1. Human resources**

All results of the automatic first pass processing on the incoming data are interactively revised and a subsequent decision is taken by technical analysts at the Centre as to whether or not there is a need to transmit messages or issue warnings. Uninterrupted operations at the Centre are warranted by having technical analysts working on three, eight-hour shifts per day. Also, on-duty technicians are available on twenty-four-hour basis, in case problems arise with computer and technical maintenance.

### **2.2. Technical resources**

#### *2.2.1. Technical monitoring*

Monitoring of the system is done automatically by computer software that constantly checks all the different parts, from the availability of servers and links that provide data, to the data storage capacity of partitioned hard disks. In case of a seismic event, an alert is sent to the analyst-in-charge, who can

then make the diagnosis of any problem and apply procedures for the monitoring process to resume normal operation.

### *2.2.2. Equipment redundancy*

To prevent, or at least minimize downtime, all critical components of the system have been duplicated and can be either automatically or manually switched from one to another, depending on the problem and the type of equipment. For the purpose of retrieving data in case the primary mean of transmission fails, all critical data have a backup link that can be used. Generally, the backup link uses the Internet.

## **2.3. Data used**

CENALT uses two kinds of data for its assessment operations: seismic and sea level data. The incoming seismic data is used to detect an earthquake, determine its epicenter and focal depth, as well as estimate its magnitude. Within the different stations used by the system, a certain number is considered as mission-critical and constitutes the backbone of the CENALT network (Figure 1). The other stations are used to further improve on the quality of results. Also, transmitted sea level data is used to detect whether a tsunami has been generated, to measure the actual time-travel of tsunami propagation through the Mediterranean Sea or the Atlantic Ocean basin and to confirm the forecast of potential tsunami wave level in the transmission of a warning.

### *2.3.1. Seismic data*

The seismic data originates from more than seventy (70) seismic stations. The data is received either through VSAT (very small aperture terminal) satellite links, or through MPLS (Multi-Protocol Label Switching) links. Backups for the French stations are GPRS (General Packet Radio Service) links. More seismic data is received from a hundred stations that are outside the backbone network, but this data is transmitted and received only through Internet links without any backup.

### *2.3.2. Sea level data*

Sea level data from a total of thirty-four (34) sea level stations (tide gauge) of the French Hydrographic and Oceanographic Service (SHOM) is transmitted through VPN (Virtual Private Network) links and around ten also through GTS (Global Telecommunication System). Sea level data of about forty stations (tide gauge) from other countries is retrieved via a direct link through the Internet and through the monitoring facility of UNESCO – IOC (Intergovernmental Oceanographic Commission). Two (2) extra sea level stations located in the Azores and Portugal also transmit sea level data through GTS links.

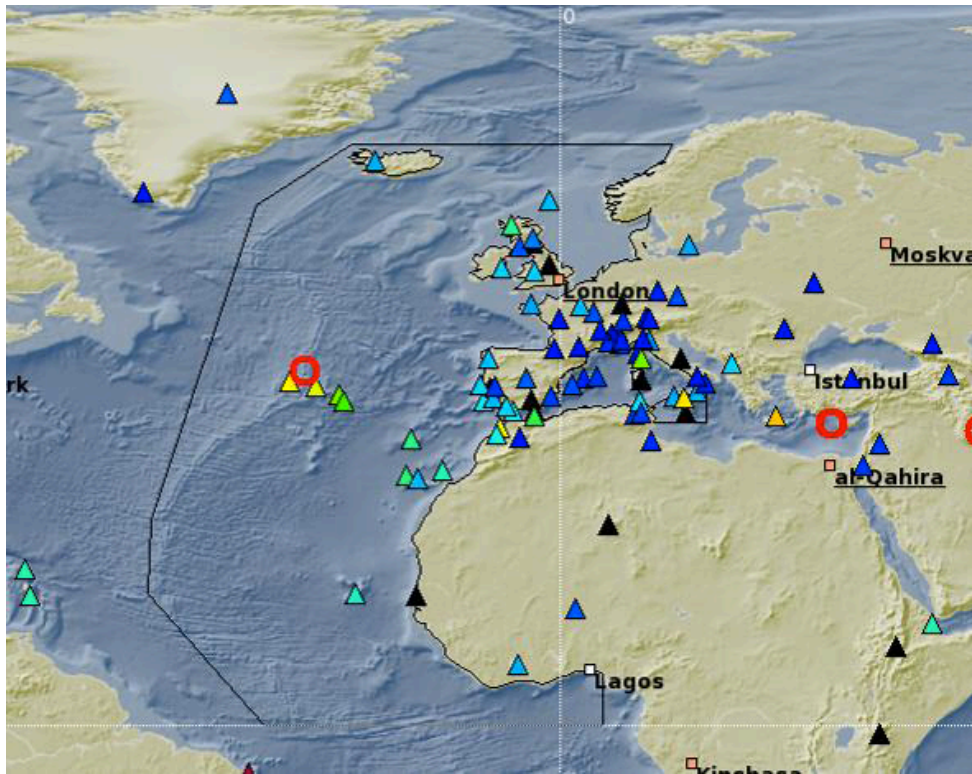


**Figure 1.** Partial map of seismic stations used by CENALT, extracted from the SeisComP3 application.

## 2.4. Data Processing

### 2.4.1. Processing of seismic data

The SeisComP3 (Seismological Communication Processor) software from Gempa is the core of the automatic detection of seismic events. The software analyses automatically the seismic data stream and locates the detected earthquake events. It then permits the interactive work of the analyst to improve the determination of the earthquake parameters.

### 2.4.2. Processing of sea level data

The Guitar software (developed by Gempa) continuously analyses the sea level data and allows measurements of the wave parameters at the participating tide gauge stations. CEA has developed, with its sub-contractors, additional software that is plugged-in in the Guitar software. One of the modules, “Cassiopée”, aggregates pre-determined tsunami scenarios to produce maps of tsunami risks. Another module, “Calypso”, calculates in near real-time the sea wave height in the deep sea, using as its basis the seismic event parameters. In case of an earthquake that could trigger a tsunami,

another software calculates the propagation time of the waves and the predicted arrival time of the first tsunami wave at the different forecast points. An example of this process is given in **Figure 2**.

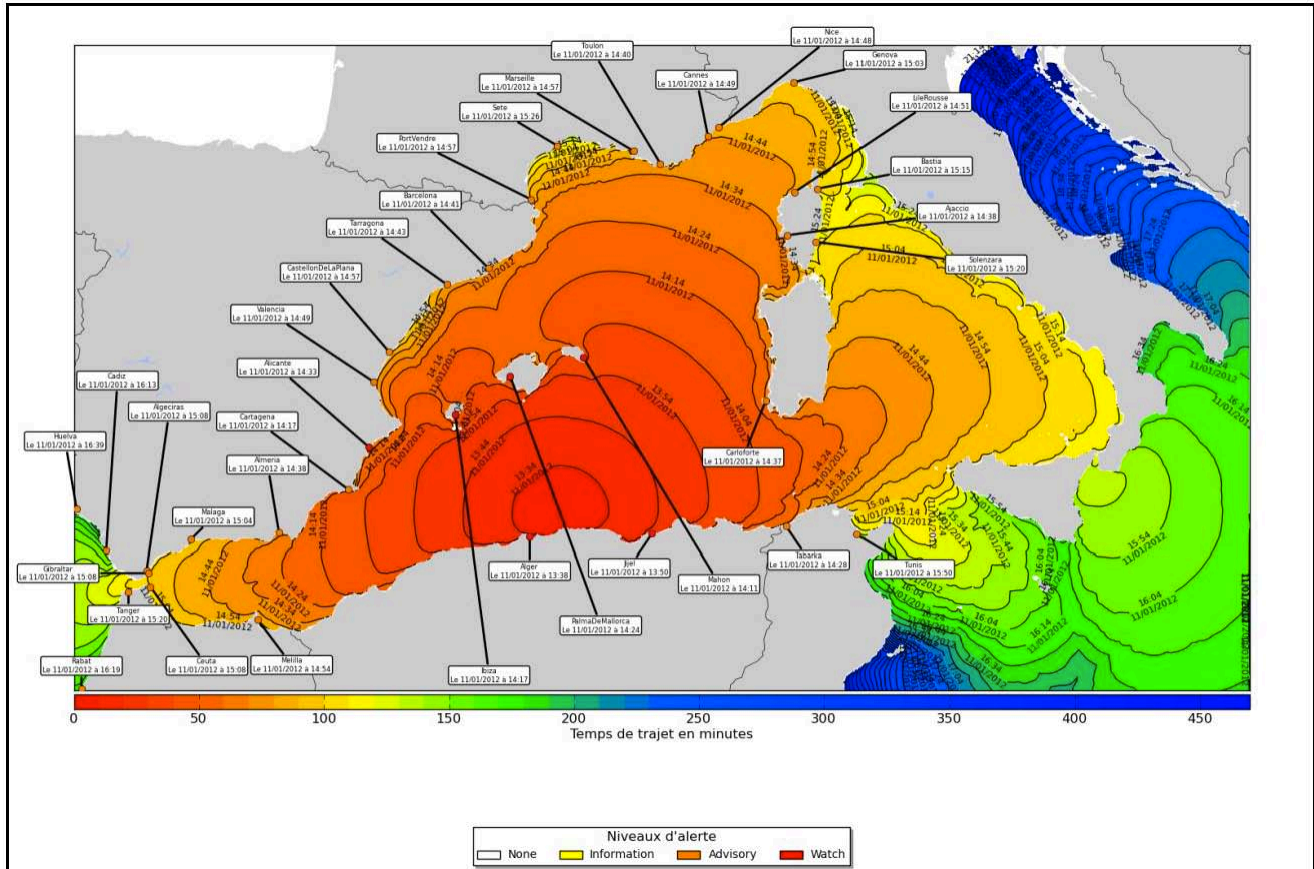


**Figure 2.** Propagation of a tsunami wave and arrival time at different forecast points for an event near the North African Margin.

## 2.5. Transmission of the information

In case of an earthquake that could potentially generate a tsunami, CENALT has both national and international responsibility to send messages to designated recipients in the region. Depending on the parameters of the seismic event, a decision matrix gives the different levels of information, warning or alert, which needs to be sent (**Figure 3** for the international matrix decision). Figure 4 indicates the different levels of warning that are issued – based on the magnitude and the region that may be affected (national or international), providing as an example an earthquake near the North African Margin.

### 2.5.1. National messages

Messages are sent to the Civil Security at the French Ministry of Interior, the Centre Opérationnel de Gestion Interministérielle des Crises (COGIC). The messages are sent through a dedicated MPLS link, as well as by e-mail and fax.

Depth	Localisation	Mw	Tsunami Potential	Type of Message
< 100 km	Offshore or close to the coast ( $\leq 40$ km inland)	5.5 à 6.0	weak potential of local tsunami	Information Message
		6.0 à 6.5	Potential of destructive local tsunami < 100 km	Regional Tsunami Advisory
	Offshore or close to the coast ( $\leq 100$ km inland)	6.5 à 7.0	Potential of destructive regional tsunami < 400 km	Regional Tsunami Watch - Basin-wide Tsunami Advisory
		$\geq 7.0$	Potential of destructive tsunami in the whole basin > 400 km	Basin-wide Tsunami Watch
	Inland (> 40 km and $\leq 100$ km)	5.5 à 6.5	weak potential of local tsunami	Information Message
$\geq 100$ km	Offshore or inland ( $\leq 100$ km)	$\geq 5.5$	Nil	Information Message

*No message if the earthquake is localized inland beyond 100 km distance*

**Figure 3.** Decision matrix for seismic event that occurs in the Mediterranean Sea.

### 2.5.2. International messages

Internationally, messages are sent by GTS, e-mail and fax to the countries which have subscribed by sending a request to the IOC. The first international communication test by CENALT was conducted on 22 May 2012. Test messages were sent to thirty-five (35) institutes in thirty-one (31) countries. E-mails and faxes were directly sent to participants and, additionally, a message was also sent by GTS. Since the beginning of operations of the Centre on the 1<sup>st</sup> of July 2012, several countries have requested through the IOC to be recipients of messages from CENALT. A first successful e-mail and fax communication test was conducted on the 8 August 2012 with these countries, to verify the correct transmission and receipt of messages. Since that time regular monthly communication tests are performed by GTS, email and fax, to an increasing number of recipients. In January 2013, 15 recipients belonging to 10 Member states and 2 international bodies received messages from CENALT.

The international activities of the CENALT were: a) the presentation of the CENALT activity report to the Intergovernmental Coordination Group (ICG) of IOC at the meeting in September 2012; b) the participation of France at the end of November 2012 to the NEAM Wave 12 tsunami exercise by providing a potential scenario; and c) the continuous integration (and tests) of contact points in the countries which have or will request receipt of messages from CENALT.

On the developmental side, rapid calculations of focal mechanisms will be implemented, tested and evaluated, to improve the efficiency of tsunami impact assessment for an event which may occur in the monitored region.

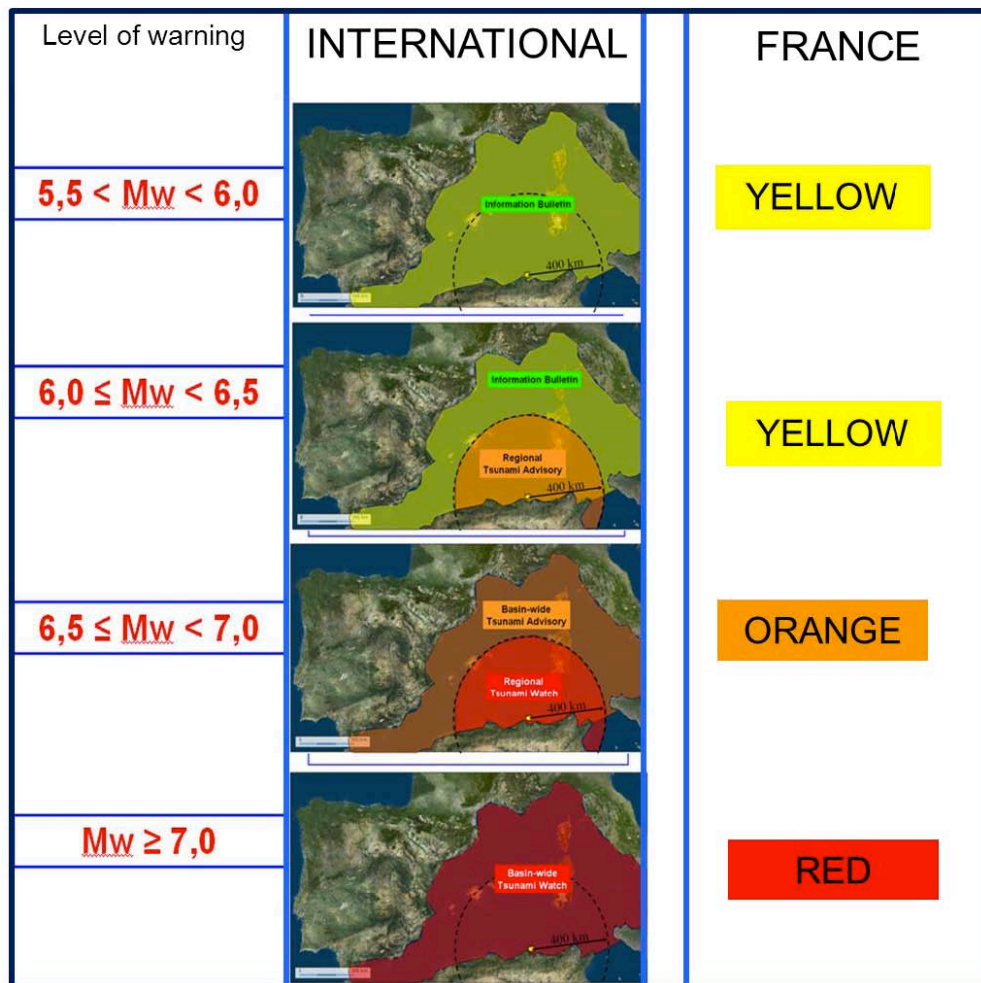
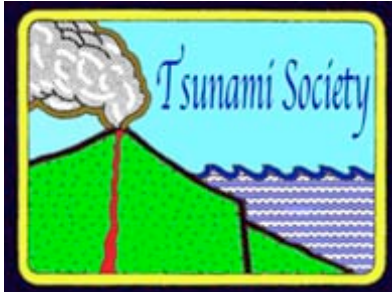


**Figure 4.** Different levels of warnings for International and National (France) regions monitored in the Western Mediterranean Sea.



## SCIENCE OF TSUNAMI HAZARDS

---

Journal of Tsunami Society International

Volume 32

Number 1

2013

---

### SEVERAL TSUNAMI SCENARIOS AT THE NORTH SEA AND THEIR CONSEQUENCES AT THE GERMAN BIGHT

**Silvia Chacón-Barrantes**

*Departamento de Física, Universidad Nacional de Costa Rica, Heredia, COSTA RICA*

*Now at the Coastal Research Laboratory, University of Kiel, GERMANY*

*email: [silviachaconb@gmail.com](mailto:silviachaconb@gmail.com)*

**Rangaswami Narayanan**

*Formerly, Reader, Department of Civil and Structural Engineering, University of Manchester, Manchester,  
UNITED KINGDOM.*

**Roberto Mayerle**

*Coastal Research Laboratory, University of Kiel, GERMANY*

#### ABSTRACT

Tsunamis occurred in the past at the North Sea, but not frequently. There are historical and geological records of several tsunamis: the Storegga tsunami caused sediment deposits in Scotland 8,000 years ago and records of at least six earthquake-generated tsunamis exist from 842 to 1761 AC. The highest tsunami height witnessed at the German Bight is comparable to the maximum storm surge recorded and could thus cause similar or higher damage. However, there is little research on tsunami modeling in the North Sea. Here, we performed ten numerical experiments imposing N-waves at the open boundaries of a North Sea model system to study the potential consequences of tsunamis for the German Bight. One of the experiments simulated the second Storegga slide tsunami, seven more explored the influence of the incidence direction of the tsunami when entering the North Sea domain, and the other two explored the influence of tides on tsunami heights. We found that the German Bight is not exempt from tsunami risk. The main impact was from waves entering the North Sea from the north, even for tsunamis with sources south of the North Sea. Waves entering from the English

Channel were attenuated after crossing the Dover strait. For some scenarios, the tsunami energy got focused directly at the Frisian Islands. The tidal phase had a strong influence on tsunami heights, although in this study the highest heights were obtained in the absence of tides. The duration of tsunamis is significantly smaller than that of storm surges, even though their flow velocities were found to be comparable or larger, thus increasing their possible damage. Therefore, tsunamis should not be dismissed as a threat at the North Sea basin and particularly at the German Bight.

**Keywords:** *Tsunami numerical modeling, 1755 Lisbon tsunami, 1929 Grand Banks tsunami, 1858 North Sea tsunami, submarine slide tsunami.*

## 1. INTRODUCTION

Tsunamis are not frequent in the North Sea; nevertheless, there is plenty of evidence of impact of tsunamis originating both inside and outside the North Sea basin. Many of the tsunamis had only local impact and were generated by slides in fjords, whereas others were of far reaching impact, caused by submarine slides and earthquakes. The most renowned tsunami in the North Sea was generated by the second Storegga submarine slide about 8,000 years ago in the Norwegian Sea (Harbitz, 1992). Besides this event, the NOAA Global Historical Tsunami Database (NGDC/WDC, 2012) includes tsunamis in Germany and Denmark in 1760 and in the United Kingdom and France in 842 and 1580 which were attributed to local earthquakes. Also, there are reports in this database for tsunamis in the United Kingdom, France and the Netherlands in 1755 and 1761 caused by earthquakes from the offshore area of Portugal in the Atlantic (NGDC/WDC, 2012).

To the authors' knowledge, two modeling studies on tsunamis in the North Sea have been performed to date – one by Borck et al. (2007) and the other one by Lehfeldt et al. (2007). Both studies obtained tsunami heights of less than 2m and therefore concluded that the tsunami risk is not high for the German Bight because of the shallow depths of the North Sea and because of the protection provided by Norway and the British Islands. Nevertheless, Newig and Kelletat (2011) put together several reports along the North Sea basin to demonstrate that there was a tsunami on 5 June 1858, which caused run-ups of up to 4m in Germany, specifically in Sylt, Helgoland and Wangerooge. Tsunami heights between 1.2 and 6m were reported also in the United Kingdom, France, the Netherlands and Denmark. There were no casualties reported because the summer season had not yet started and tourism was scarce at that time. Still, several people, mostly in fishing communities, were reported to have barely escaped the onslaught of the tsunami (Newig and Kelletat, 2011).

For their tsunami model, Borck et al. (2007) used as input “three successive positive single waves” generated by a sine-square function. The use of three solitary waves together has no physical meaning, as they are not a good representation of the leading tsunami wave. Lehfeldt et al. (2007) used a square hyperbolic secant solitary wave as input and imposed it perpendicularly at the open boundaries. Even when solitary waves are accepted as a representation of the leading tsunami wave, better results were obtained using N-waves to represent tsunamis because of their bipolarity

(Tadepalli and Synolakis, 1996). The reports of the 1858 tsunami in the English Channel draw attention to a withdrawal of the sea followed by inundation (Newig and Kelletat, 2011). Therefore, for this work, N-waves are used to represent the leading wave of tsunamis.

Our work described in this paper involved ten experiments in order to explore the tsunami risk in terms of run-up for the German Bight under a wider and more realistic approach. As it is well known, earthquakes are the most common source of tsunamis in the world and earthquake-generated tsunamis differ from those generated by landslides - both in amplitude and frequency. Consequently, we considered one case of a landslide-generated tsunami with normal incidence and seven cases of earthquake-generated tsunamis with various directions of incidence. In all these cases, tides were not considered in the modeling. To explore the role of tides on tsunami heights, we performed two more experiments which included tides in the calculations.

## 2. THE MODEL SYSTEM

For this work, we utilized a model system based in Delft3D software, which is a finite differences numerical model able to simulate coupled flow, sediment transport and morphodynamic processes. The model solves the non-linear shallow water equations using an alternating implicit scheme (Leeser et al., 2004). This package has been validated and verified for tsunami propagation and run-up (Apotsos et al., 2011a) and it has been employed in several one-dimensional tsunami studies like Apotsos et al. (2011b), (2011c), Apotsos et al. (2009) and Gelfenbaum et al. (2007), and two-dimensional tsunami studies like Vatvani et al. (2005).

Specifically for this study, we modified an existing model system which covers the entire North Sea. The model system consists of four, two-dimensional, nested models: a) the Continental Shelf Model (CSM) from Verboom et al. (1992); b) the North Sea Model (NSM) from Bruss et al. (2010); c) the German Bight (GBM); and d) the Dirthmarschen Bight (DBM) models from Hartsuiker (1997). For the present study, we employed only two models of the system, the NSM and the GBM. The first model covers only the North Sea and it is not capable of computing inundation on dry land. In this model the input waves can be imposed in both the western and the northern open boundaries. The second model, the GBM, covers the German coasts and it is capable of simulating inundation on dry land. The nesting boundaries between the NSM and the GBM are drawn with thick black lines in Figure 1. The resolution of the original NSM varies between 7079.62m and 9349.68m, and the corresponding Imamura numbers vary between 4.64 and 6.25. The Imamura number is defined as:

$$Im = \frac{dx}{2h} \sqrt{1 - gh \left( \frac{dt}{dx} \right)^2} \quad 1$$

with dx the grid resolution, dt the time step and h the water depth. The Imamura number relates numerical and physical dispersion on the modeling of tsunami propagation and it should be kept close to one (Imamura and Goto, 1988). As the Imamura numbers of the NSM are much larger than one, we refined this grid by a factor of three. The refined NSM (refNSM) has a resolution between 2359.87m

and 3116.58m. The corresponding Imamura numbers are between 0.72 and 1.57, more appropriate for tsunami propagation.

In the present work the tsunami-like waves were imposed using the Riemann-invariant boundary condition to minimize false reflections in the open boundary (Verboom and Slob, 1984). As the Riemann invariant is calculated with the water level and the flow velocity, for N-waves we used the flow velocity of the shallow water wave theory,  $U=\eta gh$ , where  $\eta$  is the water level,  $g$  is the gravity acceleration and  $h$  is the water depth. If an open boundary had no incoming wave then a zero Riemann invariant was prescribed to allow the wave leaving the domain.

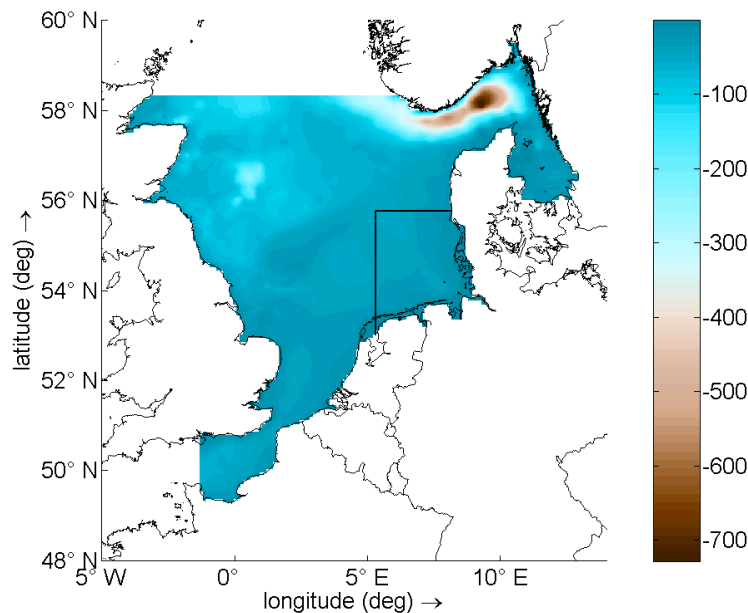


Figure 1. Extent and bathymetry of the model system. The thick black lines show the boundaries between the German Bight Model (GBM) and the North Sea Model (NSM). The color scale is in meters of depth.

### 3. VALIDATION OF REFINED MODEL

The nesting between CSM and GBM was validated by Mayerle et al. (2005), later by Bruss et al. (2010) which splitted the CSM and defined the NSM. As the NSM consists on a section of the CSM and has the same resolution, the nesting between the NSM and the GBM is the same as between the CSM and the GBM. Nevertheless, as we refined the North Sea grid for tsunami propagation purposes, the nesting between the refNSM and the GBM needed to be validated. For this purpose, we performed simulations of three large storms at the North Sea, which occurred in 1967, 1976 and 1999 with the original and refined North Sea models. Additionally, the mild weather conditions from April 2008 were simulated to include more general scenarios. To test the nesting of the refNSM with the GBM we compared its results with results from the NSM nested to the GBM, as this original nesting has been extensively validated with field data (Mayerle et al., 2005; Bruss et al., 2010).

For all validation cases, air pressure and wind fields were imposed in both North Sea models and the results were used as input, together with air pressure and wind fields, for the GBM. The percentage difference between the maximum water heights calculated by both models at the German Bight was smaller than 3% for the whole domain in all cases, indicating that the differences between results from both model systems are negligible, and that the refNSM can be nested to the GBM using the same procedure as for the original model system.

#### 4. STOREGGA-LIKE TSUNAMI

In the first tsunami experiment, we modeled the second Storegga tsunami. Harbitz (1992) modeled the tsunamis caused by the first and second Storegga slides in the Norwegian Sea 8000 years ago. His resultant time series of water level for the second slide in offshore Aberdeen, Scotland (his station 8), shows a leading depression N-wave with maximum amplitudes of about 2.5m. The time between the maximum depression and maximum elevation is about 96min. To reproduce such a wave we used the formulation of landslide N-waves by Carrier et al. (2003):

$$\eta(t) = a_1 e^{-k_1 \cdot (t-t_1)^2} - a_2 e^{-k_2 \cdot (t-t_2)^2} \quad 2$$

where  $\eta$  is the water level perturbation,  $t$  is the time, and for the constants the following values were assigned:  $a_1=2.35\text{m}$ ,  $a_2=2.61\text{m}$ ,  $k_1=0.00125\text{min}^{-1}$ ,  $k_2=0.001\text{min}^{-1}$ ,  $t_1=471\text{min}$  and  $t_2=381\text{min}$ . The resulting wave is plotted with a solid line in Figure 2. This wave matches Harbitz (1992) modeling, drawn as a dashed line in the same figure. This N-wave defined the boundary condition for a tsunami generated by a landslide, imposed normal to the northern boundary of the refNSM. No wave was imposed at the western boundary.

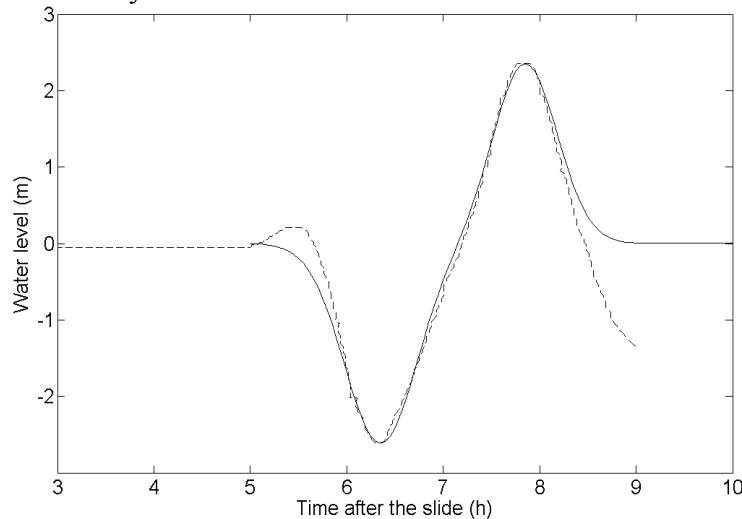


Figure 2. Water level of the N-wave imposed as boundary condition (solid line) for the Storegga-like experiment. The results from Harbitz (1992) for the second Storegga slide are shown with a dashed line.

The bathymetry used in the model during the simulations was the present bathymetry. The mean sea level nowadays is not the same as 8000 years ago, and neither is the bathymetry. Therefore, the goal of this experiment was not to obtain accurate calculations of the historical tsunami run-up but only the consequences for the German Bight if the same tsunami would happen today. As the North Sea Model is not capable in calculating the inundation of dry land, the maximum tsunami heights were computed for the offshore area. However, because of the shoaling effect, the corresponding run-ups should be expected to be larger.

Maximum water levels of more than 5m over the mean sea level were obtained at Inverness and Edinburgh (Firth of Forth), Scotland. These results match those of Smith et al. (2004) who concluded that the run-up of the second Storegga tsunami in inlets at Scotland mainland, probably exceeded 5m over the local mean high water mark of spring tides at that time, while it was probably less along the open coast. Figure 3, left side, illustrates the computed maximum tsunami heights along the entire North Sea basin, roughly confirming these estimates.

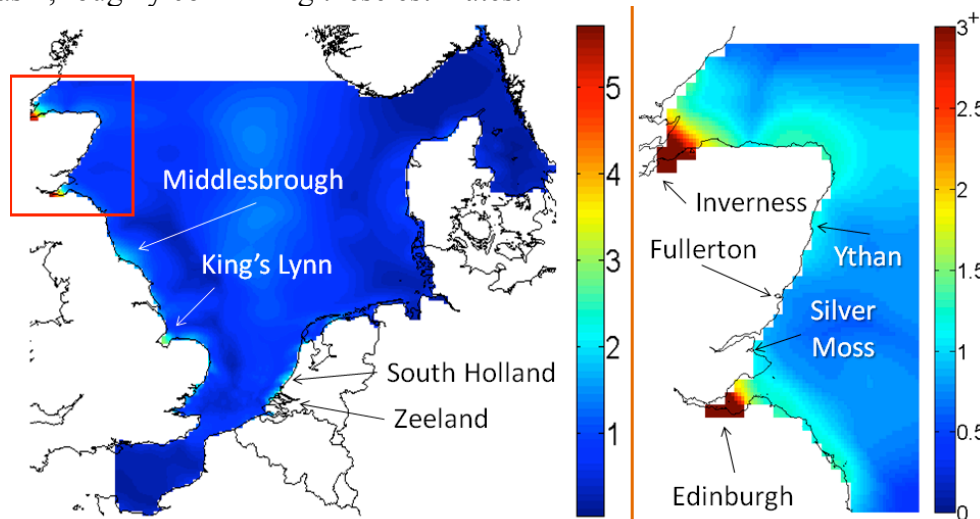


Figure 3. Left side: Maximum tsunami heights in meters at the whole North Sea basin for the Storegga-like tsunami, the red rectangle shows the detailed area at the right side where deposits from Storegga tsunami have been identified. At the right side the color scale is saturated to depict more details.

At the right hand side of Figure 3 the maximum tsunami heights are shown along the British coasts where tsunami deposits from Storegga event have been identified. At the open coast site of Waterside (mouth of the river Ythan), maximum offshore heights of 1-1.5m were obtained. Here the maximum height of the sediment deposits is also about 1-1.5m (Smith et al., 2004). According to Dawson (1999), the height of sediment deposits is lower than the maximum tsunami run-up and considering that run-up should be larger than offshore tsunami heights, our calculations are satisfactory in this point. In small inlets the model results underestimated the tsunami heights. The tsunami deposits suggest a minimum run-up of about 4m in Fullerton (Smith et al., 2004) and our model reproduces about 1m of maximum offshore tsunami height. At Silver Moss, the tsunami deposits point to a

minimum tsunami run-up of about 2m (Smith et al., 2004) and our model calculated about 1.3m of maximum offshore tsunami height. Together with the lack of correct bathymetry, there is another reason for these differences. Specifically, the refNSM does not include these inlets completely because of its resolution. Also, the refNSM does not consider inundation of dry land; therefore the interaction of the tsunami with the coast is not well solved. At small inlets this interaction determines greatly the tsunami heights. Smith et al. (2004) postulated that the Storegga tsunami also impacted the U.K. shorelines south of where the tsunami deposits were found. Our model system predicted offshore tsunami heights above 2m in places like Middlesbrough and King's Lynn (Figure 3 left side). Maximum offshore tsunami heights of over 2m were also obtained in the south coast of the Netherlands, offshore South Holland and Zeeland - although no sediment deposits have been found in these places.

Figure 4 illustrates the simulated maximum tsunami heights in the whole German Bight domain for a Storegga-like tsunami. The highest values of almost 2m were obtained for the Western Frisian Islands, specifically at Schiermonnikoog and Ameland, and smaller values of about 1m were obtained for the Northern Frisian Islands, particularly for Sylt. Figure 5 shows water level time series for the six German stations in the regions of higher tsunami heights. Among these stations, the highest water level of almost 1.0m was computed in Westerland, Sylt Island. Despite the fact that the tsunami heights seemed to be not high enough to pose a risk to German coasts, all the time series depicted in Figure 5 have a leading depression shape, which usually implies larger onshore velocities (Pritchard and Dickinson, 2008), which can cause greater damage.

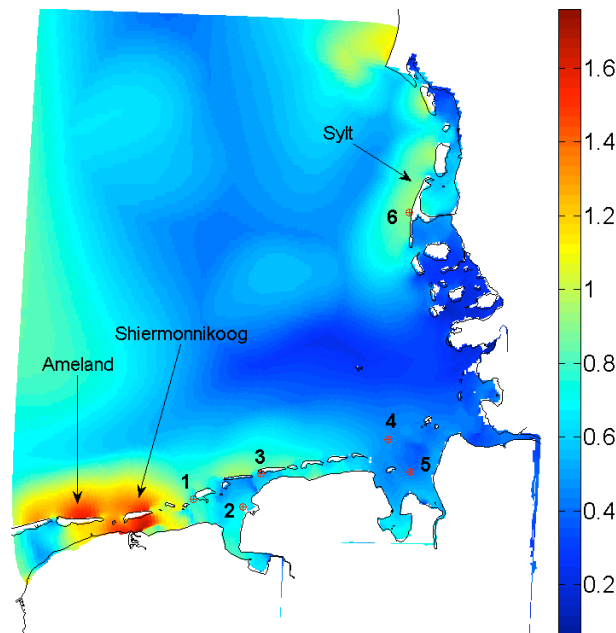


Figure 4. Simulated maximum tsunami heights in meters in the German Bight Model for the Storegga-like tsunami. The red crossed circles show the localization of the German stations where the highest tsunami heights were obtained: 1. Borkum, 2. Leybucht, 3. Norderney, 4. Alte Weser, 5. Dwarsgat and 6. Westerland.

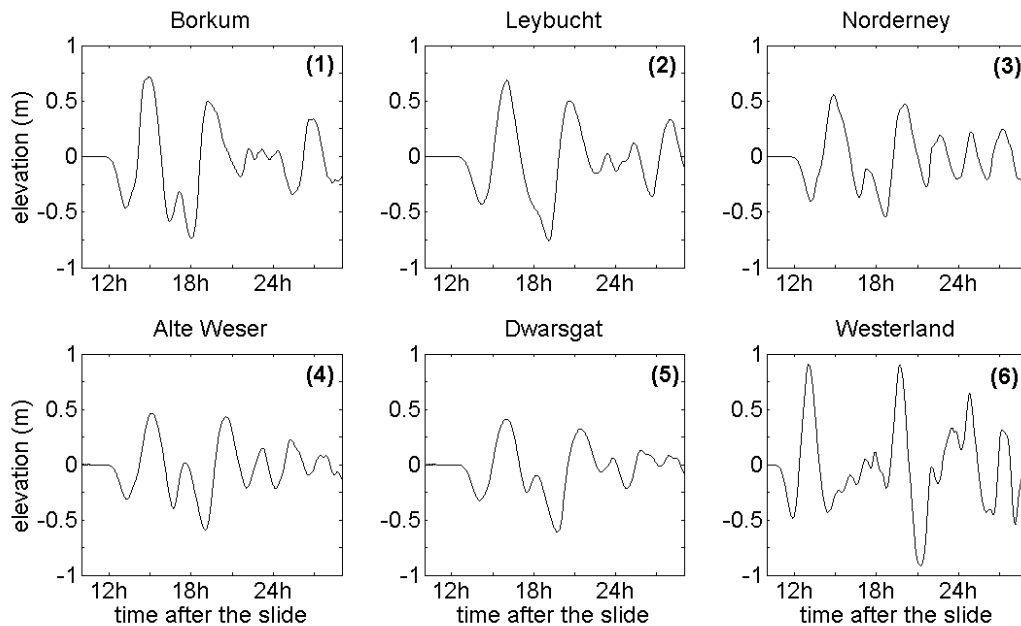


Figure 5. Simulated time series of tsunami heights at six stations on the German coast for the Storegga-like tsunami. The localization of the stations is shown in Figure 4. The time is given in hours after the event and in all plots water elevation is given in meters over the mean sea level.

## 5. EARTHQUAKE-GENERATED TSUNAMIS

The risk of earthquake-generated tsunamis was evaluated in separate experiments, using different forcing functions from a landslide-generated tsunami. First, we considered the case of the wave entering only from the western boundary. Additionally, we considered six different directions of incidence for the wave at the northern boundary, to explore the effect of incidence directions on the focusing of the tsunami energy and the many possible sources for earthquake-generated tsunamis. Two of the incidence directions that were used corresponded to the historical 1755 Lisbon and the 1929 Grand Banks tsunamis. Earthquakes generated both of these tsunamis, however in the case of Grand Banks, the earthquake was followed by a submarine landslide.

For all the cases considered in this section, we used symmetric leading depression N-waves as input, similar to the Tadepalli and Synolakis (1996) formulation:

$$\eta(t) = \frac{3\sqrt{3}}{2} H \cdot \text{sech}^2[\gamma(t - t_0)] \cdot \tanh[\gamma(t - t_0)] \quad 3$$

In Eq. 3  $\eta$  is the water level perturbation,  $H$  is the wave height,  $t$  is time,  $t_0$  is the midpoint of the wave,  $\gamma = \frac{3}{2} \alpha \cdot \sqrt[4]{\frac{3}{4} A}$  and  $\alpha$  is a constant which determines the width of the wave. Because of

the date of the tsunamis referred above, no data is available on the height or the width of the incoming waves. Nevertheless, for the 1858 event, the water was reported to recede and then come back in 5-7min, in Bologne-sur-Mer and in Le Havre, in the English Channel. Consequently, we chose  $t_0=20\text{min}$  and  $\gamma=0.2087\text{min}^{-1}$  to have 6min between the depression and the peak of the N-wave. Although N-waves are non-periodic waves, Synolakis et al. (2008) define an equivalent wavelength as the distance between the points where the wave height is 1% of its maximum value at the beginning and at the end of the N-wave. Using this definition, the equivalent period of our wave was 33.2min, typical of the earthquake-generated tsunamis. A unitary height was used for the incoming waves because the goal of this section was to identify the vulnerable regions and the wave height amplification.

## 6. IMPACT OF THE WESTERN WAVE

In this experiment, the wave was imposed only at the western boundary of the refNSM (Figure 1). Tsunami heights of 1-2m were obtained at Bognor Regis at the English Channel (not shown). By comparing wave heights before and after crossing the Dover Strait, the western wave was highly attenuated after passing through this strait. The wave just before and just after crossing the strait is shown in Figure 6, at points with similar depths of about 36m. The maximum heights after crossing the strait were less than half of those before crossing. With an incoming wave of unitary height at the mouth of the English Channel, the maximum wave height after the Dover strait was about 10cm. This strong damping implies that there should be almost no interference between a wave entering the domain through the west and a wave entering the domain through the north.

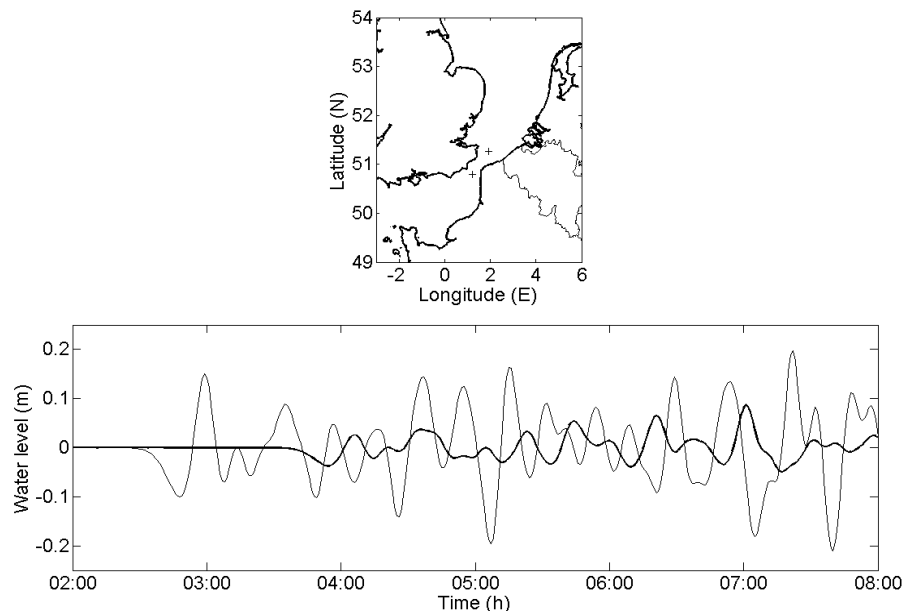


Figure 6. Bottom: Comparison of the western wave just before (thin line) and just after (bold line) crossing the Dover strait. Top: Location of the points where the wave was calculated. Both points have depths of around 36m.

## 6.1 Influence of the direction of incidence of the northern wave

We considered two scenarios of earthquake-generated tsunamis based on the NOAA travel time maps of the 1755 Lisbon and 1929 Grand Banks events plotted in Figure 7 (NGDC, 2012). Other authors propose different locations for the 1755 Lisbon earthquake, as usually happens for large earthquakes. In this case in particular, there were no seismograms recorded that contribute to locate the event. These two historical tsunami scenarios differed only in the incidence direction of the wave through the northern boundary. This difference can be seen in Figure 7; the Lisbon tsunami originally came from the south and travelled around Ireland before entering the northern North Sea. The Grand Banks tsunami, on the other hand, came straight from the west, crossing the North Atlantic Ocean before entering the North Sea.

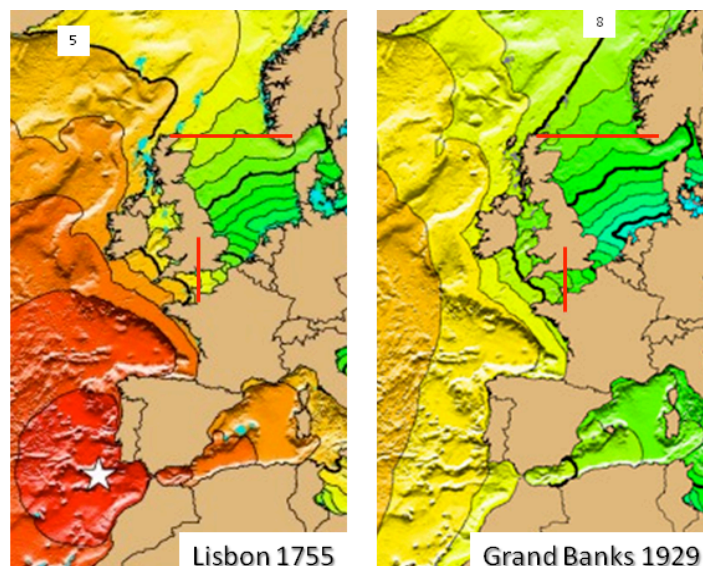


Figure 7. Travel time maps for two historical events arriving to the North Sea taken from the National Geophysical Data Center Tsunami Travel Time Maps website (NGDC, 2012). Time contours are plotted every hour and thick black lines are plotted every five hours (left) and every four hours (right). The numbers represent hours after each earthquake. Red thick lines show the approximate boundaries of the refNSM. The plots contain no information on the tsunami heights, only on its travel times.

As the depth of water along the north open boundary of the refNSM is not uniform, the incidence angle is not the same along this boundary (see time contours at Figure 7) and it is not possible to refer to a wave incidence angle for the various cases. Instead, the direction of incidence of the tsunami was given by means of the difference of arrival times between Wick in Scotland and Rekefjord in Norwegian shores, hereafter referred to as the time of entrance ( $T_e$ ). If a wave enters normally to the open boundary then the elapsed time is zero because it reaches Scotland and Norwegian shores at the same time. Following Figure 7, the time of entrance was  $T_e=183\text{min}$  ( $=3\text{h}3\text{min}$ ) for the Lisbon-like scenario, and  $T_e=122\text{min}$  ( $=2\text{h}2\text{min}$ ) for the Grand Banks-like scenario. Additionally to these two historical tsunamis, hereafter case (d) and case (c) respectively, we considered four complementary

incidence directions: normal incidence, case (a), and entrance times of 61, 244 and 305min, cases (b), (e) and (f) respectively. For simplicity we decided not to impose waves at the English Channel in this Section, as the results from Section 5.1 showed that a wave entering through the English Channel got highly damped after crossing the Dover strait. Finally, the height of the incoming wave was set to one, in order to present the results in terms of wave amplification rather than in terms of absolute wave height. We found that the incidence direction determined the places where the energy was concentrated. In the North Sea, the higher the time of entrance, the further east the focusing of wave energy (Fig. 8).

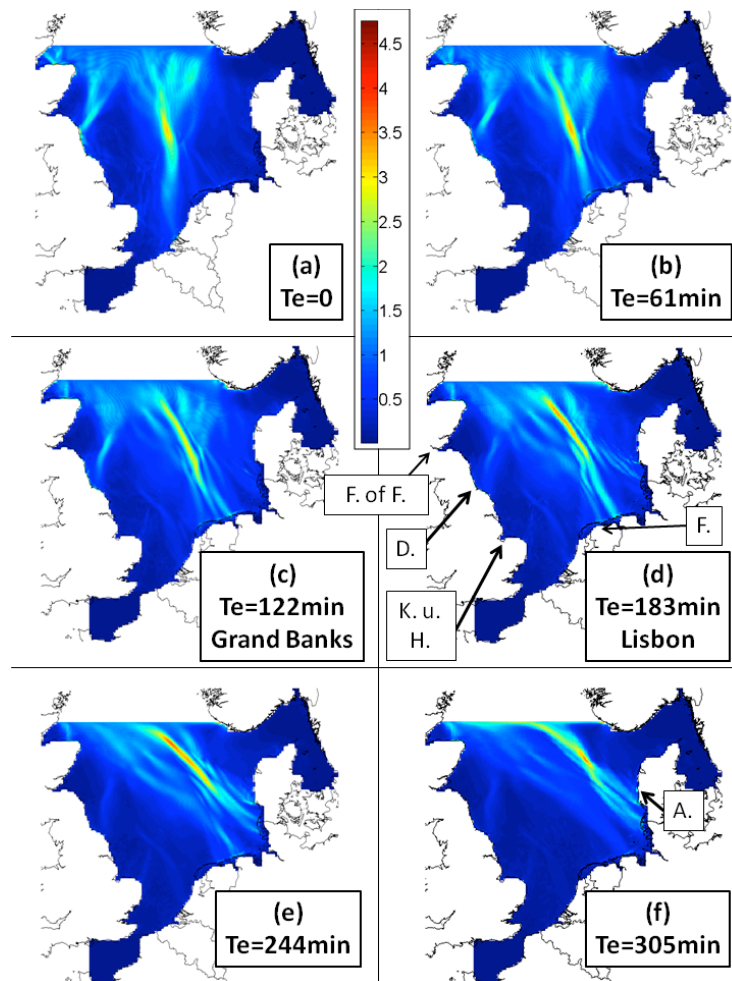


Figure 8. Maximum tsunami amplification factor for different directions of incidence of a unitary N-wave following Tadepalli and Synolakis (1996). Case (a) corresponds to perpendicular incidence. The others have oblique incidence with (b) 61min, (c) 122min (Grand Banks like), (d) 183min (Lisbon like), (e) 244min and (f) 305min time to complete the entrance through the northern boundary. Some geographical places are shown in subfigure (d): Firth of Forth (F. of F.) in Scotland, Durham (D.) and Kingston upon Hull (K. u. H.) in England, and Friesland (F.) in The Netherlands. In subfigure (f) Årgab in Denmark is pointed out.

For all the cases, a certain amount of energy was focused always on the Frisian Islands and North Sunderland in England, although the proportion depended highly on the incidence direction. For all the cases studied in this section, the tsunami heights west of the Dover Straits were negligible.

Important differences were also found due to the forcing type employed. Normal incidence (case a) affected mostly the southern coast of the Netherlands and North Sunderland in England. The Storegga-like tsunami simulated in Section 4 also arrived normal to the north open boundary and affected mostly inlets along Scotland and England.

For the Grand Banks-like tsunami (case c), most of the energy was focused on the East and West Frisian Islands and less on the Durham shores, in England (Figure 8c). For this tsunami, there were no reports of arrival in Germany, Great Britain or France. It is quite possible that the tsunami was significantly damped after crossing the Atlantic Ocean. For the Lisbon-like tsunami (case d), most of the energy was focused on the East Frisian Islands in Germany (Figure 8d). Little energy was focused to the West and North Frisian Islands in the Netherlands, Germany and Denmark and even less to the Durham shores in England. The Global Historical Tsunami Database (NGDC/WDC, 2012) reported the arrival of the Lisbon tsunami at several locations along the east coast of Great Britain, including Firth of Forth in Scotland and Durham and Kingston upon Hull in England. Damaged boats and broken moorings were reported in Friesland, the Netherlands. There are no reports of the tsunami arrival to Germany. Considering the date, the lack of reports might be also due to scarce coastal population or poor record preservation.

At the GBM, the case of completely normal incidence, case (a), presented wave heights of less than one meter, meaning no amplification of the original wave that entered at the North Sea. Case (b) with almost normal incidence, presented the lowest amplification of wave height for the GBM, of less than two. The Lisbon-like scenario (case d) presented the highest amplification among all cases, of more than three times at the north shores of Borkum and Juist Islands. The Borkum station is facing the mud flat behind the island and the water heights computed there were of less than 2m (Figure 10), corresponding to less than twofold amplification. The Westerland station, at the western shore of Sylt Island, registered the highest heights for case (e), which had more tangential incidence than the Lisbon-like case, of almost 2m as shown in Figure 10e.

The seaside of the Frisian Islands presented the highest water levels in all cases (Figure 9), yet the mudflats between the Frisian Islands and the mainland mitigated the impact of the tsunami at continental shores. This mitigation did not happen for the Storegga-like tsunami of Section 4 (Figure 4), another difference due to the waveform. The four cases of more normal incidence (cases a, b, c, and d) presented pronounced focusing of energy to the East Frisian Islands, and the two cases of more tangential incidence (cases e and f) presented more focusing of energy to the North Frisian Islands. The arrival time at each station increased with the incidence direction (Figure 10), the arrival time for the most tangential case (case f) was between 3 and 4 hours higher than for the normal incidence case (case a).

Comparing the results from the two historical tsunamis, the Grand Banks-like tsunami (case c)

presented water heights bellow those for the Lisbon-like tsunami (case d). As we employed incident waves of unitary height in all the cases, it is not only the smaller distance travelled by the tsunami what would make a Lisbon-like tsunami more dangerous than a Grand Banks-like tsunami for the German Bight, but also the orientation of its arrival at the North Sea.

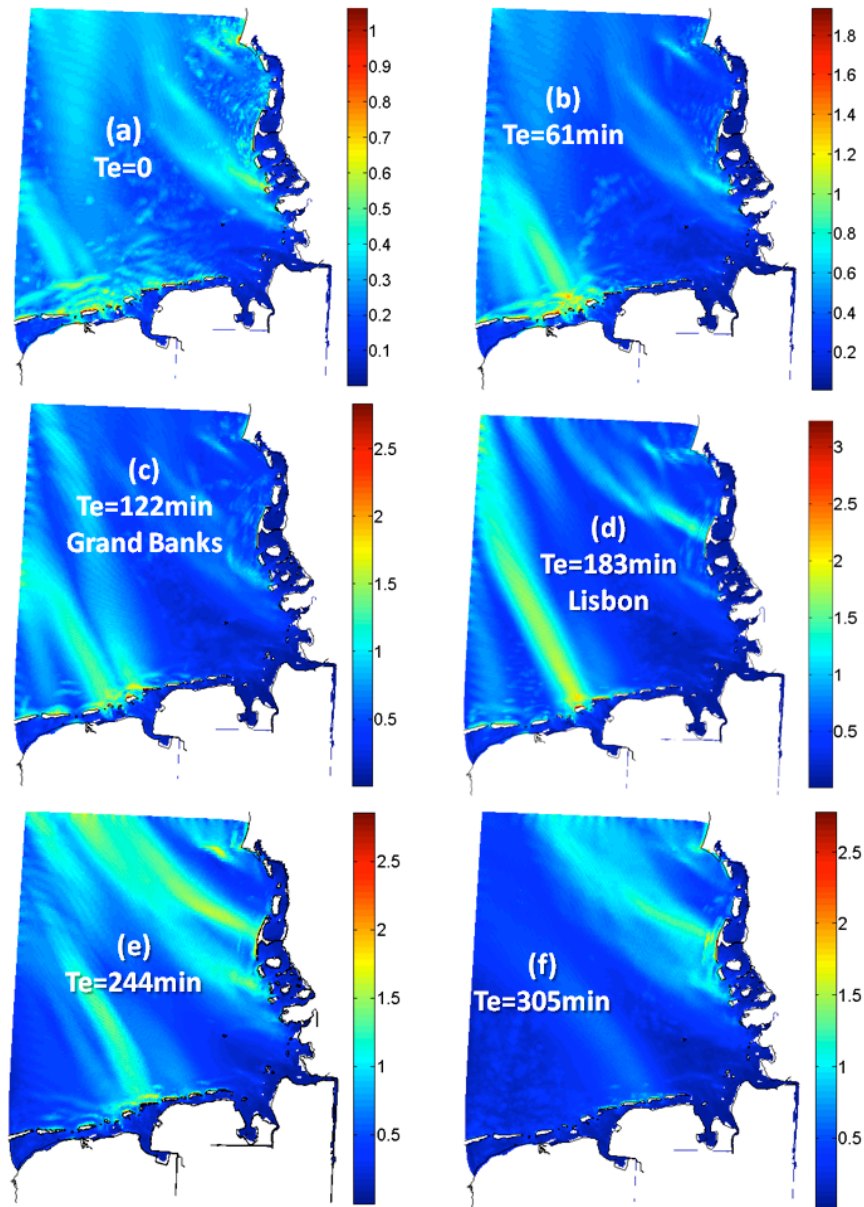


Figure 9. Maximum tsunami heights at the German Bight domain in meters for the various directions of incidence at the refined North Sea Model plotted in Figure 8. Case (a) corresponds to normal incidence. The others have oblique incidence with (b) 61min, (c) 122min (Grand Banks like), (d) 183min (Lisbon like), (e) 244min and (f) 305min time to complete the entrance through the northern boundary of the refined North Sea Model.

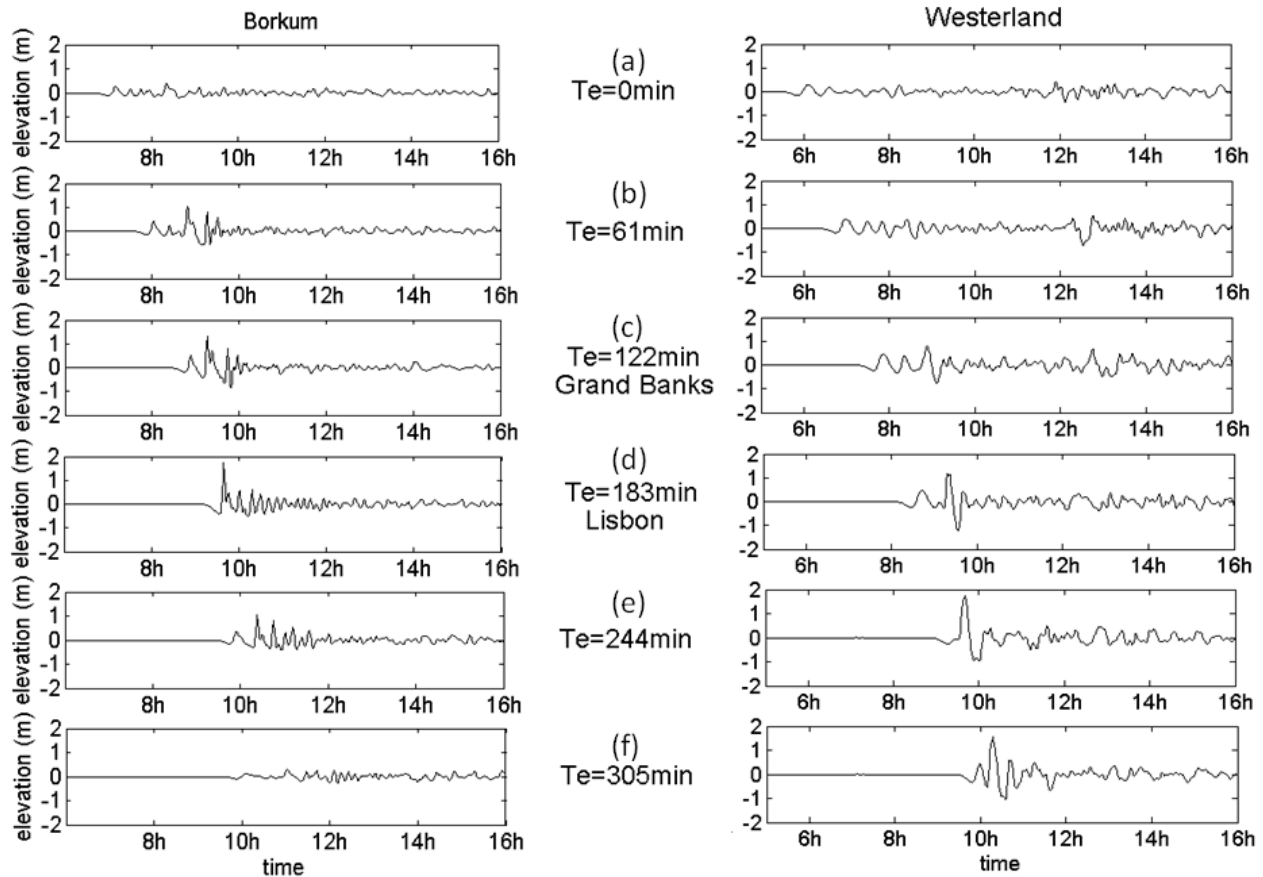


Figure 10. Time series of water height in meters for two stations at the Eastern (left) and Northern (right) Frisian Islands for the six incidence directions through the northern boundary of the refNSM.

## 7. THE 1858 NORTH SEA TSUNAMI

In 1858 a tsunami arrived to the North Sea from an unknown source. The highest water heights were reported at Wangerooge, East Frisian Islands (between 3.3 to 4m) and Westerland, Sylt Island (3.5 to 4m) in Germany, and at Blåvandshuk (4.5 to 5m) and Årgab (about 6m) in Denmark (Newig and Kelletat, 2011). There were a large number of reports of this tsunami along the English Channel, some of them of about 2.5m height. Yet the tsunami reports in Belgium and in the south of the Netherlands mention only about 1.25m height (Newig, 2012).

Newig and Kelletat (2011) conclude that the source of this tsunami was not in the English Channel itself but south of its entrance. They infer that the large tsunami run-ups in Germany and Denmark for the 1858 tsunami were due to the interference between the western wave (coming from the English

Channel) and the northern wave (coming from Scotland). Still, they recognize that the reports of tsunami heights were larger for the North Sea than for the English Channel. Our results from Section 5.1 agreed with these reports showing high damping of the Channel wave, therefore the interference as cause of larger run-up in Denmark and Germany, is unlikely. Additionally, the tsunami was reported to arrive in Germany about one hour later than in Denmark; therefore the higher run-ups in these countries were due to a wave coming from the north.

Among our results of Section 4 in the GBM, the maximum tsunami heights for the (e) and (f) cases were located at the north coast of East Frisian Islands, at the west coast of Sylt Island, both in Germany and at Blåvandshuk in Denmark (Figure 9e and Figure 9f). Årgab lays outside of the GBM so we were not able to produce a good estimation of the maximum tsunami height there. Nevertheless, the refNSM results showed high tsunami heights offshore Årgab for cases (e) and (f), higher for the later than for the former (compare Figure 8e and Figure 8f). The differences in arrival times at those three locations for case (f) also matched better the 1858 reports than for case (e), Figure 11.

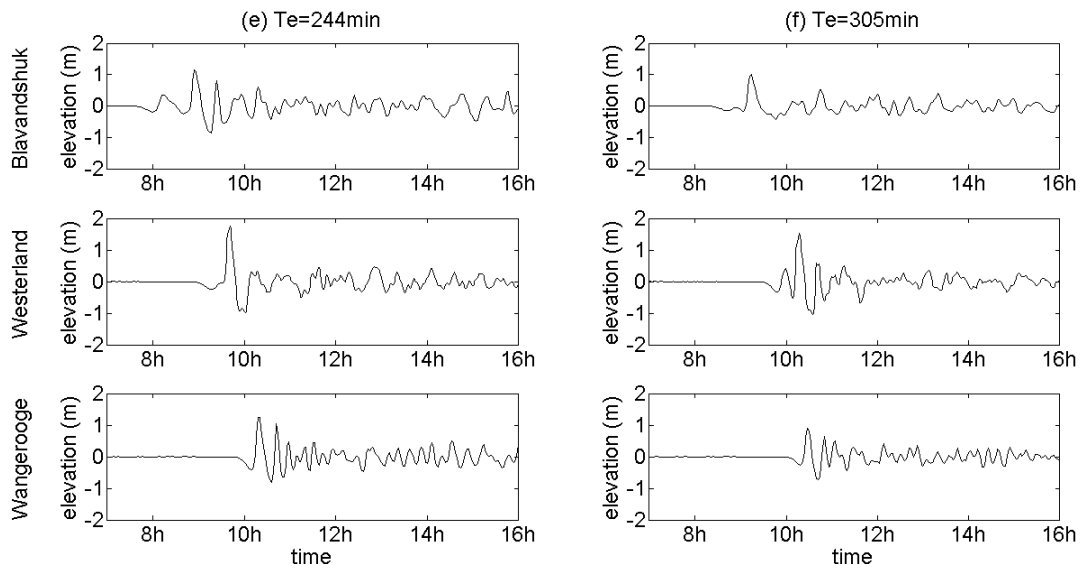


Figure 11. Time series of water height, in meters, on Blåvandshuk (Denmark), Westerland and Wangerooge (German Frisian Islands) for cases (e) and (f) of Section 5.2.

The leading depression of the tsunami wave at Blåvandshuk, Westerland and Wangerooge stations (Figure 11) was much smaller than the subsequent elevation; this could be the reason for no leading depression reported by eyewitnesses in those places (Newig and Kelletat, 2011). The reports of the 1858 tsunami run-up are higher for Blåvandshuk than for Westerland and Wangerooge, and our model system obtained higher runups for Westerland than for the other two places. The difference may be due to inaccuracies in the witnesses' reports, or the tide at the moment the tsunami arrived. We performed a simple analysis of the influence of tides on tsunami heights in Section 7 and found that they were affected by the tidal phase.

The timeline and wave height of the tsunami observations and our modeling results point that the wave that arrived in the south of the Netherlands was probably the damped western wave and it was too small to be noticed at German shores. Few hours later, the northern wave arrived to Denmark and then to Germany, with a direction of incidence similar to case (f), corresponding to an origin further east of the 1755 tsunami source given by NOAA (NGDC, 2012): 36°N and 11°W. Other authors propose epicentres further east for the 1755 earthquake, for example Moreira (1989), Reid (1914) and Zitellini (1999), all at 10°W. Also, the tsunami source could have been at Biscay Bay or offshore from Morocco.

Horsburgh et al. (2008) simulated several scenarios of tsunamis arriving at the United Kingdom shores from the offshore region of the Iberia Peninsula. They concluded that the Galician Rise shields Ireland and the west coast of Great Britain and also that the extent of the continental shelf dissipates energy of tsunamis coming from the south before they reach these coasts. However, they did not model the tsunamis at Scotland or their entrance to the North Sea. From the arrival time chart of the 1755 Lisbon tsunami (NGDC, 2012) we know that tsunamis coming from the south propagate north along the continental slope and through the Rockall Trough at high velocities, and then get refracted around Scotland and enter the North Sea. As the propagation along the continental slope and the Rockall Trough occur at great ocean depths, it is very likely that this wave experiences very little energy loss.

## **8. COMPARISON OF STORM SURGES AND TSUNAMIS**

Storms are common phenomena in the North Sea. The surges they provoke have caused inundations and damages at the German coast, thus dikes have been built along the entire coastline to protect the coastal population. Tsunamis, on the other hand, are much less frequent and they are not taken into account in preventive measures and are not present in people's memory, either.

In Figure 12, we compare the water levels and depth-averaged flow velocities caused by storm surges and tsunamis at Westerland station, on Sylt Island, because this station presented the highest heights on all the tsunami simulations performed as described in previous sections. We plotted the storm surges of February 1967, January 1976 and December 1999, which were simulated as part of the validation in Section 3. For tsunamis, we plotted the Storegga like tsunami modeled in Section 4, and the case (f) of Section 5.2. Storm surges have much larger durations than the two tsunamis shown in the paper. Although landslide-generated tsunami had larger duration and period than earthquake-generated tsunami, their duration is still much shorter than that of storm surges.

The heights for the Storegga tsunami were about half than those for the storm surges. The tsunami wave of Section 5.2 was also smaller than the storm surges, yet it was generated employing a wave of unitary height at the refNSM boundary; therefore if the incoming wave is higher, this tsunami wave could be also higher. Additionally, the magnitude of the depth-averaged flow velocity for this tsunami was about double than for storm surges. The maximum magnitude of depth-averaged flow velocity for case (f) of Section 5.2 was of 1.6m/s, for the Storegga tsunami was of 0.48m/s and for the 1967, 1976 and 1999 storm surges was of 0.74, 0.68 and 0.61m/s respectively. Then, even when the tsunamis last

much less and their water levels are smaller, their flow velocities can be larger than the storm surges causing more damage.

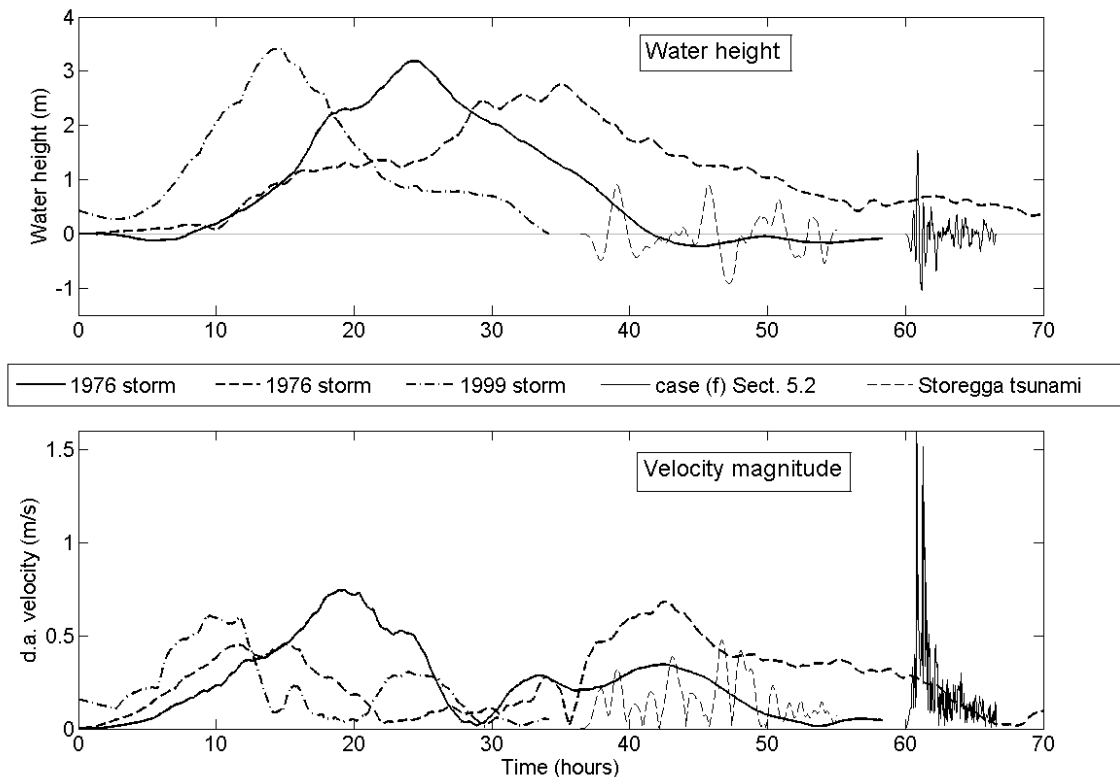


Figure 12. Comparison of storm surges and tsunamis on Westerland station, Sylt Island. The upper panel plots water levels and the bottom panel plots depth-averaged flow velocity magnitude. The times were shifted to show the differences more clearly.

## 9. TSUNAMIS AND TIDES

Tides have been proven to have an impact on storm surges in the North Sea (Bruss et al., 2010). Tsunamis are usually modeled without considering tidal influence; however, tides have been also proven to impact on tsunami heights (Kowalik et al., 2006) and (Kowalik and Proshutinsky, 2010). Kowalik and Proshutinsky (2010) superimposed tsunami signals on different stages of the tide on a simple slope channel to explore the influence of tides on tsunamis. The largest tsunami heights resulted during ebbing and low tide, because the change in bottom friction due to the interaction of tsunami and tides was larger at those stages. They conclude that under real conditions, the interaction of tsunami and tides is non-linear and it is given in terms of bottom friction, advection and momentum flux along with changing depths and velocities. Finally, they recommend tides to be simulated together with tsunamis in places where the former are comparable to prevailing depths, as it is the case for the North Sea. Therefore we superimposed an N-wave to the spring tide of August 14th 1999 to explore the influence of tides on tsunamis heights. To obtain the tidal forcing for the refNSM, we

imposed an astronomical forcing at the open boundaries of a larger model: the Continental Shelf Model (CSM) of Verboom et al. (1992). The resulting water levels and current velocities at the refNSM boundaries were used to obtain the Riemann-invariant boundary condition for 9 days of simulation. The N-wave of Section 5.2, case (a) of normal incidence, was superimposed to the tides on two different moments, such that the tsunami arrived at Cuxhaven station during high tide and low tide. This procedure was only performed for the north open boundary, on the west open boundary only the tide was prescribed. Then, the tide was subtracted from the model results of the sum of tides and tsunami, and this residual was compared with the tsunami results of Section 5.2 case (a) at Cuxhaven station. If the interaction between tsunamis and tides were linear, the residual should be equal to the tsunami modeled alone.

The results for the two cases, high tide and low tide, are compared in Figure 13: pure tsunami with thin lines and tsunami under the influence of tides with thick lines. The influence of tides and its phase on tsunami heights was remarkable. The differences between the pure tsunami and the tide-influenced tsunami were higher if the tsunami arrived during low tide than if it arrived during high tide, agreeing with the results from Kowalik and Proshutinsky (2010) for tsunamis and Bruss et al. (2010) for storm surges. However, despite the tidal phase, the pure tsunami signal presented higher heights than the tide-influenced tsunami. It is not possible to predict a tsunami event and therefore it is not possible to superimpose the right tide forcing when tsunamis are simulated. In this case, the modeling of the tsunami alone could be considered as a reasonable approximation to the maximum possible tsunami height at Cuxhaven. Still, to generalize this result more research would be desirable considering other tidal phases, tsunami frequencies and heights, and locations along the German Bight.

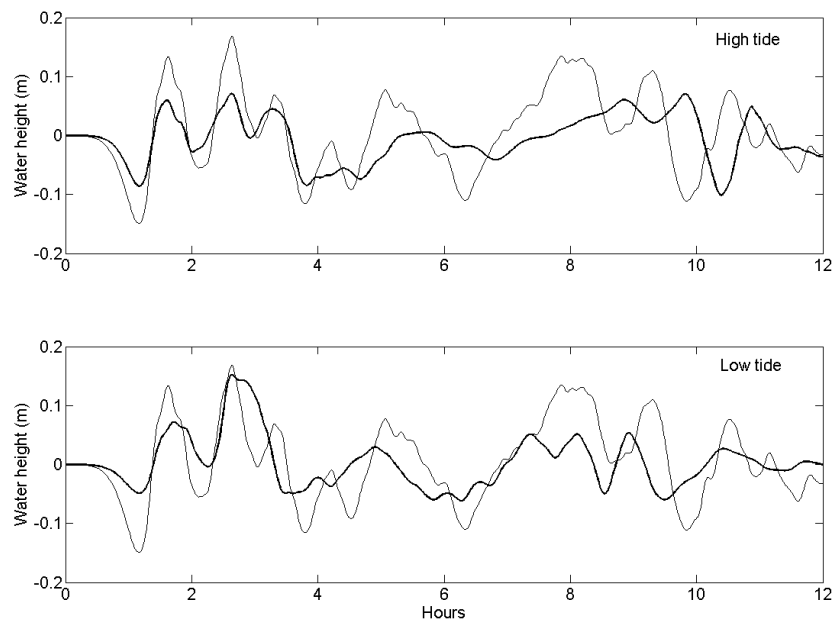


Figure 13. Influence of tides and tidal phase on tsunamis. Comparison of tsunami heights obtained without considering tides (thin line) and tsunami heights obtained taking tides into account (thick line).

## 10. CONCLUSIONS

Tsunami risk in the North Sea was explored by means of N-waves imposed at the open boundaries of the refined North Sea model. Each tsunami affected different regions on the North Sea basin and the German Bight. For the German Bight, among all cases analyzed, the most dangerous tsunamis were those generated by earthquakes south of the North Sea, because of their incidence direction. Particularly for the 1858 tsunami, the location of the most affected regions and their arrival times along the German Bight and Denmark were well reproduced. Our results indicated that the reason for the highest heights reported for this tsunami in this region was directionality rather than wave interference. This directionality points to a source for this tsunami further east from the Gorringer Banks.

The type of tsunami source was found to play an important role determining the most affected regions. Submarine slides generated tsunamis and earthquake generated tsunamis differ not only in their characteristic amplitudes but also in frequency and shape. Those differences were remarkable as the Storegga-like tsunami and an earthquake generated tsunami imposed in the same way affected different regions in the German Bight and the North Sea.

The interaction of tsunamis and tides was tested using one tsunami case in two tidal phases. The results showed that for the North Sea this interaction is clearly non-linear. The tsunami heights were higher for the tsunami arriving during low tide; however the tsunami heights without considering tides were the highest ones. More experiments considering other tidal phases, tsunami characteristics and stations would be necessary to generalize this result.

The highest tsunami heights reported in history at the German Bight are about 4m, comparable to the maximum storm surge recorded at this region. However, it was found that the depth-averaged flow velocity generated by tsunamis was comparable or larger than that generated by storm surges, suggesting that a large tsunami may cause more damage than a storm surge. Therefore, tsunamis should not be dismissed as a threat for the German Bight.

## REFERENCES

- Apotsos, A., Buckley, M., Gelfenbaum, J., Jaffe, B. and Vatvani, D. (2011a), Nearshore tsunami inundation model validation: towards sediment transport applications, *Pure and Applied Geophysics*, doi:10.1007/ss00024-011-0291-5.
- Apotsos, A., Gelfenbaum, G. and Jaffe, B. (2011b), Process-based modeling of tsunami inundation and sediment transport, *Journal of Geophysical Research - Earth Surface*, 116, (F01006), doi:10.1029/2010JF001797.
- Apotsos, A., Jaffe, B. and Gelfenbaum, G. (2011c), Wave characteristic and morphologic effects on the onshore hydrodynamic response of tsunamis, *Coastal Engineering*, 58, 1034-1048, doi:10.1016/j.coastaleng.2011.06.002.
- Apotsos, A., Jaffe, B., Gelfenbaum, G. and Elias, E. 2009, 'Modeling time-varying tsunami sediment deposition', *Proceedings of Coastal Dynamics 2009*, Tokyo, doi:10.1145/9789814282475\_0037.
- Borck, I., Dick, S., Kleine, E. and Müller-Navarra, E. 2007, 'Tsunami - a study regarding North Sea coast', Nr. 41/2007, Bundesamt für Seeschifffahrt und Hydrographie, Hamburg and Rostock.
- Bruss, G., Gönnert, G. and Mayerle, R. 2010, 'Extreme scenarios at the German North Sea Coast. A numerical model study.', *Coastal Engineering*, Shanghai, China.
- Carrier, G.F, Wu, T.T and Yeh, H. (2003), Tsunami run-up and draw-down on a plane beach, *Journal of Fluid Mechanics*, 475, 79-99.
- Dawson, A.G. (1999), Linking tsunami deposits, submarine slides and offshore earthquakes, *Quaternary International*, 60, 119-126.
- Gelfenbaum, G., Vatvani, D., Jaffe, B. and Dekker, F. 2007, 'Tsunami inundation and sediment transport in vicinity of coastal mangrove forest', *Coastal Sediments 2007*, American Society of Civil Engineers (ASCE), New Orleans.
- Harbitz, C.B (1992), Model simulations of tsunamis generated by the Storegga Slides, *Marine Geology*, 105, 1-21.
- Hartsuiker, G. 1997, 'Deutsche Bucht and Dirthmarscher Bucht, Set-up and Calibration of Tidal Flow Models', *Delft Hydraulics*, Report H1821, Delft.
- Horsburgh, K.J, Wilson, C., Baptie, B.J, Cooper, A., Cresswell, D., Musson, R.M.W, Ottemöller, L., Richardson, S. and Sargeant, S.L (2008), Impact of a Lisbon-type tsunami on the U.K. coastline and the implications for tsunami propagation over broad continental shelves, *Journal of Geophysical Research*, 113, C04007, doi:10.1029/2007JC004425.
- Imamura, F. and Goto, C. (1988), Truncation error in numerical tsunami simulation by the finite differences method, *Coastal Engineering in Japan*, 31, 245-263.
- Kowalik, Z. and Proshutinsky, A. (2010), Tsunami-tide interactions: a Cook Inlet case study, *Continental shelf research*, 30, 633-642, doi:10.1016/j.csr.2009.10.004.
- Kowalik, Z., Proshutinsky, T. and Proshutinsky, A. (2006), Tide-tsunami interactions, *Science of Tsunami Hazards*, 24:4, 242-256.
- Leeser, G.R., Roelvink, J.A, van Kester, J.A.TM and Stelling, G.S (2004), Development and validation of a three-dimensional morphological model, *Coastal Engineering*, 51, 883-915.
- Lehfeldt, R., Milbradt, P., Plüss, A. and Schüttrumpf, H. (2007), Propagation of a Tsunami-Wave in the North Sea, *Die Küste*, 72, 105-123.

- Mayerle, R., Wilkens, J., Escobar, C. and Windupranata, W. (2005), Hydrodynamic Forcing Along the Open Sea Boundaries of Small-Scale Coastal Models, *Die Küste. Archive for research and technology on the North Sea and Baltic Coast*, 69, 203-228.
- Moreira, V.S 1989, 'Seismicity of the Portuguese continental margin', in S Gregersen, PW Basham (eds.), *Earthquakes at North Atlantic Passive Margins Neotectonic and Postglacial Rebound*, Kluwer, Massachusetts.
- NEWIG, J. 2012. Personal Communication.
- Newig, J. and Kelletat, D. (2011), The North Sea tsunami of June 5, 1858, *Journal of Coastal Research*, 27:5, 931-941, doi:10.2112/JCOASTRES-D-10-00098.1.
- NGDC. 2012. Tsunami Travel Time Maps. [online]. [Accessed 2012].  
<[http://www.ngdc.noaa.gov/hazard/tsu\\_travel\\_time.shtml](http://www.ngdc.noaa.gov/hazard/tsu_travel_time.shtml)>
- NGDC/WDC 2012, Global Historical Tsunami Database, viewed 2012,  
<[http://www.ngdc.noaa.gov/hazard/tsu\\_db.shtml](http://www.ngdc.noaa.gov/hazard/tsu_db.shtml)>.
- Pritchard, D. and Dickinson, L. (2008), Modelling the sedimentary signature of long waves on coasts: implications for tsunami reconstruction, *Sedimentary Geology*, 206, 42-57, doi:10.1016/j.sedgeo.2008.03.004.
- Reid, H.F (1914), The Lisbon earthquake of November 1 1755, *Bull. Seismological Society of America*, 4, 53-80.
- Smith, D.E, Shi, S., Cullingford, R.A, Dawson, A.G, Dawson, S., Firth, C.R, Foster, I.DL, Fretwall, P.T, Haggart, B.A, Holloway, L.K and Long, D. (2004), The Holocene Storegga Slide tsunami in the United Kingdom, *Quaternary Science Reviews*, 23, 2291-2321, doi:10.1016/j.quascirev.2004.04.001.
- Synolakis, C.E, Bernard, E.N, Titov, V.V, Kanoglu, U. and Gonzalez, F.I (2008), Validation and Verification of Tsunami Numerical Models, *Pure and Applied Geophysics*, 165, 2197-2228.
- Tadepalli, S. and Synolakis, C.E. (1996), Model for the leading waves of tsunamis, *Physical Review Letters*, 77:10, 2141-2144.
- Vatvani, D., Boon, J. and Ramanamurty, P. 2005, 'Flood risk due to tsunami and tropical cyclones and the effect of tsunami excitations on tsunami propagations', *Proc. of the IAEA Workshop on External Flooding Hazards at NNPS, Kalpakkam - Tamil Nadu*.
- Verboom, G., Ronde, J. and Dijk, R. (1992), A fine grid tidal flow and storm surge model of the North Sea., *Continental Shelf Research*, 12:2, 213-233.
- Verboom, G.K and Slob, A. (1984), Weakly-reactive boundary conditions for two-dimensional water flow problems, *Advances in water resources*, 7:4, 192-197.
- Zitellini, N., Chierici, F., Sartori, R. and Torelli, L. (1999), The tectonic source of the 1755 earthquake and tsunami, *Ann. Geofis.*, 42, 49-55



**ASSESSMENT OF TSUNAMI GENERATION POTENTIAL THROUGH RAPID ANALYSIS  
OF SEISMIC PARAMETERS**

**Case study: Comparison of the Sumatra Earthquakes  
of 6 April and 25 October 2010**

**Madlazim**

*Physics Department, Faculty of Mathematics and Sciences, Surabaya State University  
(UNESA) Jl. Ketintang, Surabaya 60231, INDONESIA.  
e-mail: [m\\_lazim@physics.its.ac.id](mailto:m_lazim@physics.its.ac.id)*

**ABSTRACT**

The purpose of the research was to estimate P-wave rupture durations ( $T_{dur}$ ), dominant periods ( $T_d$ ) and rupture durations greater than 50 seconds ( $T_{50Ex}$ ) for two large, shallow earthquakes, which occurred off the coast of Sumatra on 6 April and 25 October 2010. Although both earthquakes had similar parameters of magnitude and focal depth, the 25 October event ( $M_w=7.8$ ) generated a tsunami while the 6 April event ( $M_w=7.8$ ) did not. Analysis of the above stated parameters helped understand the mechanisms of tsunami generation of these two earthquakes. Measurements from vertical component broadband P-wave quake velocity records and determination of the above stated parameters could provide a direct procedure for assessing rapidly the potential for tsunami generation. The results of the present study and the analysis of the seismic parameters helped explain why one event generated a tsunami, while the other one did not.

**Keywords:** *P-wave; rupture duration; dominant period; rupture duration greater than 50 seconds; direct procedure.*

## 1. INTRODUCTION

Seismological agencies such as the Japan Meteorology Agency (JMA), the Indonesian Tsunami Early Warning System (Ina-TEWS), the Tsunami Warning Center of West Coast/Alaska (WCATWC) and the Pacific Tsunami Warning Center (PTWC), measure and determine quickly earthquake parameters of location, depth and magnitude. Based on assigned threshold limits for earthquakes that have the potential to generate a tsunami with a height of 0.5 meters or more, JMA provides a warning for Japan in about three minutes after the origin time (OT). Similarly applying the same earthquake threshold criteria, Ina-TEWS provides early warning in about five minutes after OT. Both WCATWC and PTWC issue tsunami warnings in about five to ten minutes after OT, for shallow, North America and Pacific earthquakes, which have magnitudes greater than ( $M_w \geq 7.5$ ). In spite of the fact that all warnings that are issued by these centers are based on earthquake parameters that meet criteria of location, depth  $< 70$  km and magnitude  $> 7$ , not all such earthquakes generate tsunamis and some of the warnings that may be issued are improperly labeled as “false”. However, none of the warnings issued in real-time can be considered as false. There is simply not sufficient seismic data in real-time to assess the tsunami potential of each event. Thus, a method that can help evaluate an event’s additional, initial seismic parameters, may lead to better assessment of its potential for the generation of a destructive tsunami.

The present study was undertaken to evaluate two large, shallow earthquakes, which occurred off the coast of Sumatra on 6 April and 25 October 2010. Although both earthquakes had similar parameters of magnitude and focal depth, the 25 October event ( $M_w=7.8$ ) generated a tsunami while the 6 April event ( $M_w=7.8$ ) did not.

## 2. SEISMIC SETTING AND EARTHQUAKE PARAMETERS

Indonesia is one of the most seismically active zones on earth. Most earthquakes near the Sunda Trench are shallow, but deeper earthquakes also occur along the Benioff/Wadati zone as the Australia-Indian Plate subducts beneath the Sunda micro-plate. Figure 1 shows the historic seismic activity from 1997 to 2012 near the epicenters of the two earthquakes of 6 April and 25 October 2010. Both of these earthquakes fit well the pattern of focal depths that occur near the subsurface boundary of Australia-Indian tectonic plate and of the Sunda microplate.

As shown in Figure 1, the Centroid Moment Tensors (CMT) of both 2010 events had almost identical CMT parameters. However the 25 October earthquake generated a tsunami while the 6 April event did not. Although, moment magnitude ( $M_w$ ) is usually a good discriminant for many earthquakes as to their potential for tsunami generation, events characterized as “tsunami earthquakes, can generate larger tsunami waves than would be expected from just their moment magnitude (Kanamori, 1972; Satake, 2002; Polet & Kanamori, 2009; Lomax & Michelini, 2011).

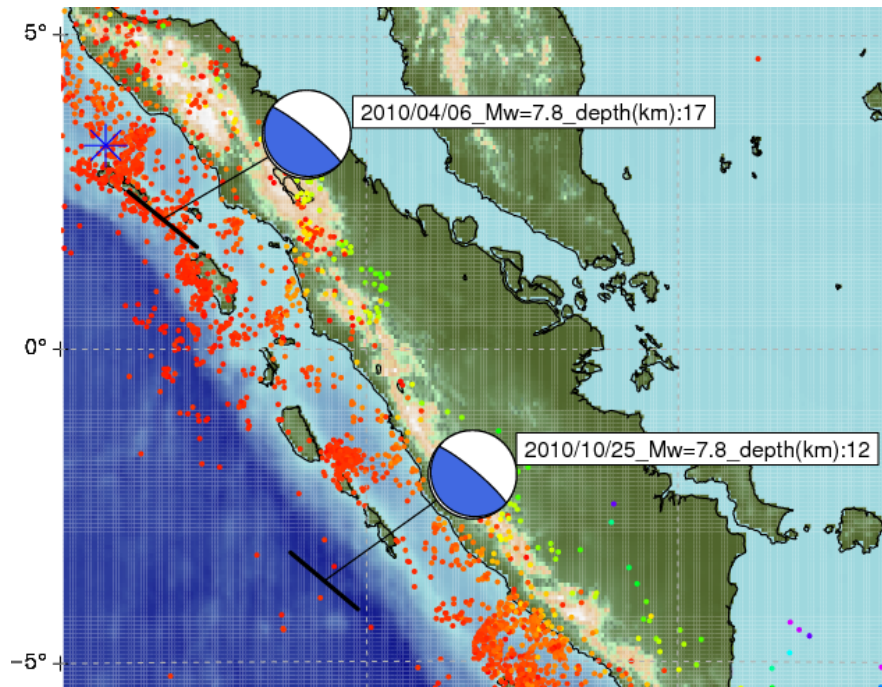


Figure 1. Centroid Moment Tensors (CMT) of the 6 April and 25 October 2010 earthquakes. Both events were shallow, had magnitudes of  $M_w=7.8$  and reverse focal mechanism.

(<http://www.globalcmt.org/CMTsearch.html>). <Figure produced by using CRAN-R and GEOMAP (Madlazim, 2010; Lees, 2012)>.

The potential for tsunami generation by an shallow focus earthquake near the coast or at sea, relates to its seafloor crustal displacements, which depend on length  $L$ , width  $W$ , mean slip  $D$ , (LWD) and depth,  $z$ , of an earthquake's rupture. Correlation between LWD and  $M_0$  can be written as:

$$M_0 = \mu LWD$$

or

$$LWD = M_0/\mu,$$

where  $\mu$  is the shear modulus at the source. The seafloor displacement and thus tsunami potential should scale with:

$$LWD = M_0/\mu.$$

If  $\mu$  is taken as constant for all shallow earthquakes,  $M_0$  and the corresponding  $M_w$  should be good discriminants for tsunami potential; indeed, for a point source, the tsunami wave amplitude is expected to be directly proportional to  $M_0$  (Okal 1988). These effects can cause an underestimate by

$M_w$  of an effective  $LWD$  value to explain the observed tsunami waves (Okal, 1988; Satake, 1994; Geist and Bilek, 2001; Lay and Bilek, 2007; Polet and Kanamori, 2009; Lomax and Michelini, 2011). To estimate  $M_w$  one cannot use a direct procedure, but may use an indirect procedure. However  $LWD$  can be estimated by using a direct procedure (Madlazim, 2011a, b, c, d).

$T_{50Ex}$  and  $T_{dur}$ , have good correlation to the tsunami size measures because  $T_{50Ex}$  and  $T_{dur}$  is related directly to a component of the  $LWD$  source - the rupture length

$$L: T_{dur} \propto L/v_r,$$

where  $v_r$  is the rupture velocity (Lomax and Michelini, 2009; Lomax and Michelini, 2011; Madlazim, 2011b). Furthermore,  $v_r$  with  $S$ -wave velocity and shear modulus  $\mu$ , increases with depth while  $v_r$  is found to be very low at shallow depth for tsunami earthquakes (Geist and Bilek, 2001; Polet and Kanamori, 2009; Lomax and Michelini, 2011). The dominant period  $T_d$ , as the peak  $\tau_c$  value is obtained is applied with a 5 second sliding time window from 0 to 55 seconds after  $P$  wave arrival (Lomax and Michelini, 2011). The definition of  $T_d$  follows from assessment of numerous possible parameters with the goal of better discrimination of a tsunamigenic earthquake. The value of 5 seconds for the time window is sufficient to identify if  $T_d$  is greater or less than about 10 seconds.

The present study measured  $P$ -wave rupture duration ( $T_{dur}$ ), dominant period ( $T_d$ ) and rupture duration greater than 50 second ( $T_{50Ex}$ ) for the two large Sumatra earthquakes as recorded by the vertical components of seismographs, for the purpose of describing why the 25 October event ( $M_w=7.8$ ) generated a tsunami while the 6 April event ( $M_w=7.8$ ) did not.

### 3. DATA

The research criteria for the analysis of the two Sumatra earthquakes were: (1) what occurred after 2008 on the data available by the GEOFON-BMKG network; (2) the centroid depth was shallow ( $\leq 20$  km); (3) the moment magnitudes in the Global CMT catalog of both earthquakes are almost identical at 7.8; (4) the half duration is almost the same at about 20 seconds; (5) the focal mechanism types are almost the same (reverse). The CMT parameters of the earthquakes are shown in Figure 1 and Table 1 below. In conducting the investigation, we retrieved BHZ channel waveforms of the GEOFON-BMKG network stations for these earthquakes from GEOFON-BMKG (Fig. 2). As described in Madlazim (2011b), data was used from the stations within the epicentral distance ranging from  $4^\circ - 15^\circ$ . This was done in order to avoid scattering due to the upper mantle or D structures (Shearer and Earle, 2004; Hara, 2007).

Table 1. Comparison of CMT parameters of the 6 April and 25 October 2010 Sumatra earthquakes

Event	Lat	Long	Depth	St1; St2	Dp1; Dp2	Sl1; Sl2	Mw	HD (s)
2010/04/06 22:15	2.07	96.74	17.6	307; 129	7; 83	88; 90	7.8	19.5
2010/10/25 14:42	3.71	99.32	12.0	316; 130	8; 82	98; 89	7.8	19.9

(<http://www.globalcmt.org/>). St1: strike 1, Dp1: dip 1. Sl1: slip 1, HD: Half duration

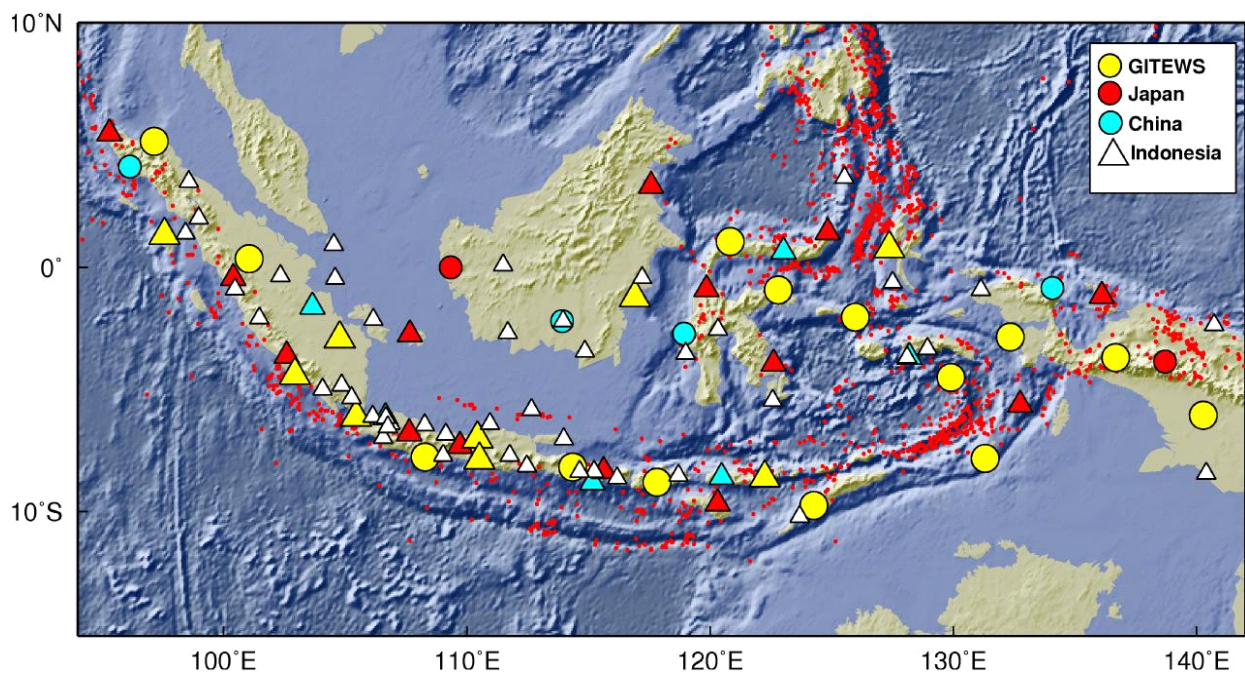


Figure 2. Stations used to estimate  $T_{dur}$ ,  $T_d$  and  $T_{50Ex}$  for the 6 April and 25 October 2010 earthquakes. ([www.fdsn.org/meetings/.../fdsn\\_indoc\\_net.ppt](http://www.fdsn.org/meetings/.../fdsn_indoc_net.ppt))

#### 4. METHOD

We determined  $T_{dur}$  for the earthquakes, through high-frequency (HF) analysis of the vertical-component, broadband seismograms as described in the literature (Lomax and Michelini, 2005; Lomax et al., 2007; Lomax and Michelini, 2009; Lomax and Michelini, 2011; Madlazim, 2011b).  $T_d$  The estimation was done by using direct procedure, namely: (1) by refining the vertical component velocity seismograms recorded by the GEOFON-BMKG networks by using a Butterworth filter at high frequency (5 - 20 Hz); (2) by picking the arrival time of the P wave automatically; (3) by integrating the vertical component velocity seismograms and comparing with the vertical component

acceleration seismograms, multiplied by  $2\pi$ ; and (4) by the value of  $T_d$  which is the culmination of the results of such integration. For estimating  $T_{50Ex}$  we used a direct procedure by the following steps: (1) to (2) the same as those estimated  $T_d$ ; (3) by calculating the rms amplitude ( $A_r$ ) and  $T_{50}$ ; and (4) by calculating  $T_{50Ex}$  which is a comparison between  $T_{50}/A_r$ . Figure 3 and 4 are flow charts which outline the direct procedure of P-wave dominant period and  $T_{50Ex}$ , respectively.

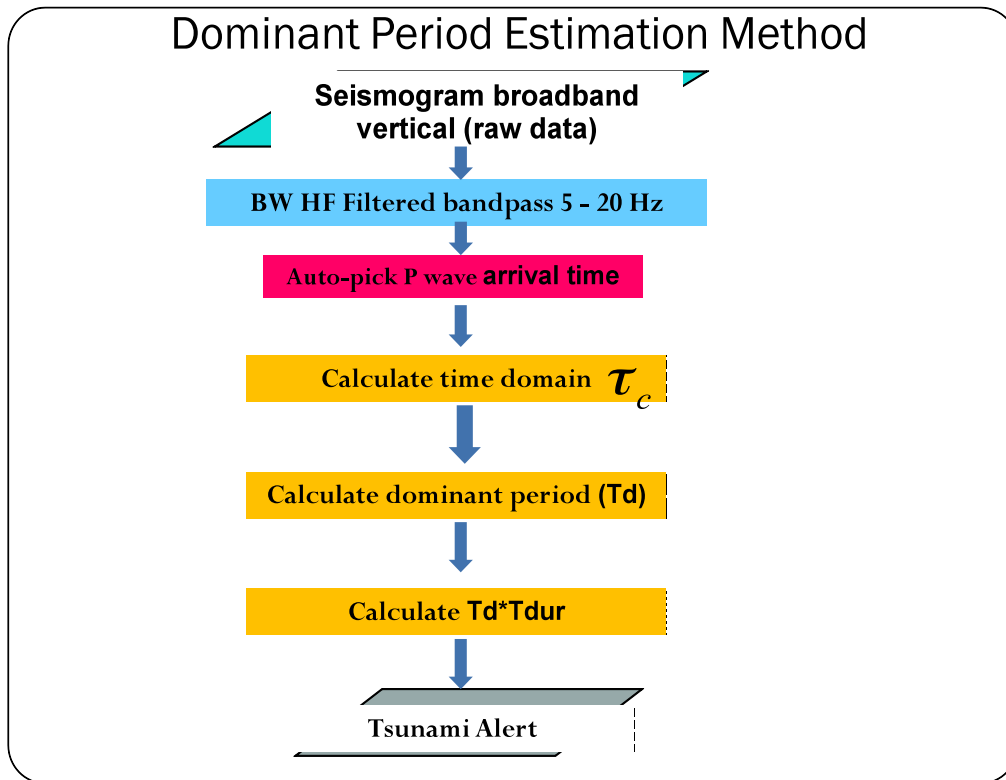


Figure 3. Direct procedure to estimate P-wave dominant periods

The importance of Tsunami generation “ $I_t$ ”, of the two Sumatra earthquakes was determined based on 0 - 4 descriptive indices “ $I$ ”, of tsunami effects (deaths, injuries, damage, houses destroyed), and maximum water height “ $h$ ” in meters from the NOAA/WDC Historical Tsunami Database ([http://www.ngdc.noaa.gov/hazard/tsu\\_db.shtml](http://www.ngdc.noaa.gov/hazard/tsu_db.shtml)) in order to determine the potential of earthquake tsunami generation, where:

$$I_t = i_{\text{height}} + i_{\text{deaths}} + i_{\text{injuries}} + i_{\text{damage}} + i_{\text{houses-destroyed}}$$

where  $i_{\text{height}} = 4, 3, 2, 1, 0$  for  $h = 10, 3, 0.5$  m,  $h > 0$  m,  $h = 0$  m respectively (Lomax and Michelini, 2009). Based on this equation, we got values of  $I_t = 1$  (no tsunami) for the 6 April 2010 earthquake and  $I_t = 13$  (tsunami) for the 25 October 2010, event.

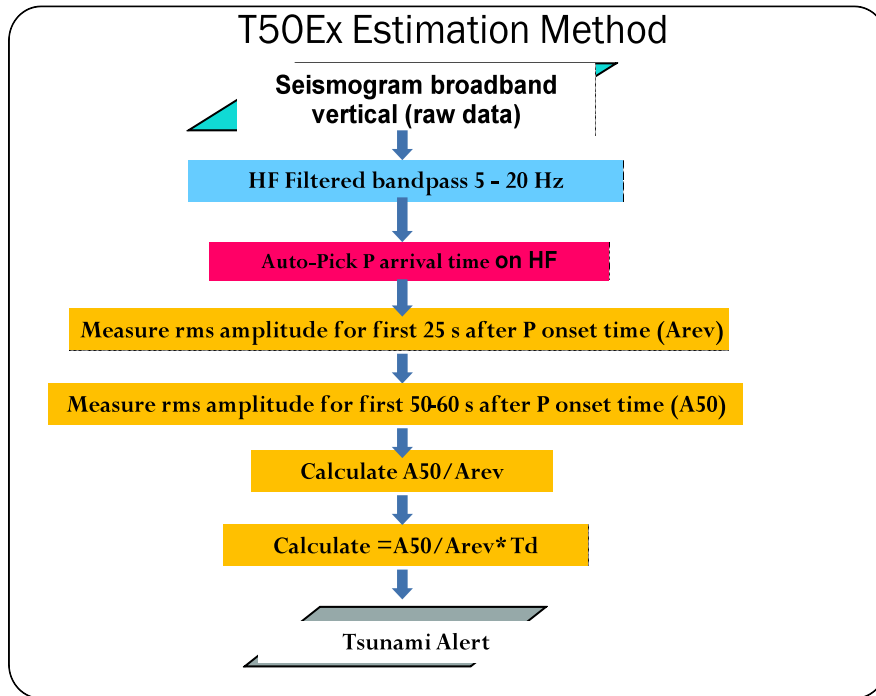


Figure 4. Direct procedure to estimate P-wave T50Ex

## 5. RESULTS AND DISCUSSION

The discriminant tsunami potential  $T_{dur}T_d$  and  $T_dT50Ex$  correctly identified for the two tsunamigenic events with  $I_t = 13$  (tsunami),  $M_w = 7.8$  for the 25 October event and  $I_t = 1$  (no tsunami),  $M_w = 7.8$  for the 6 April event (Table 2)., more than the  $M_w$  and  $T_{dur}$  only discriminants (Lomax and Michelini, 2011; Madlazim, 2011). This result evaluated for the 6 April event in my previous study, did not use this methodology.

Table 2. Analysis result of discriminants tsunami potential by using the direct procedure

Event	Lat	Lon	Depth (km)	Fault type	$M_w$	$T_{dur}$	$T_d$	T50Ex	$T_{dur}T_d$	$T_dT50Ex$	$I_t$
20100406	2.07	96.74	17.6	Reverse	7.8	116	3.1	0.9	359	2.79	1
20101025	-3.71	99.32	12.0	Reverse	7.8	136	8.7	1.5	945	13.2	13

Discriminant tsunami potential  $T_{dur}$ ,  $T_d$  and  $T_d T_{50Ex}$  critical threshold for 6 April 2010 event,  $T_{dur} T_d < 550 \text{ s}^2$  and  $T_d T_{50Ex} < 10 \text{ s}^2$  (no tsunami), respectively would provide important complementary information to initial location, depth and magnitude estimates for early assessment of earthquake tsunami potential. Since  $T_d$  is obtained rapidly ( $< 60 \text{ s}$ ) after the  $P$  arrival, it remains to rapidly assess  $T_{dur}$  for an earthquake, in particular if  $T_{dur} > 55 \text{ s}$ ,  $T_d < 10 \text{ s}$  and  $T_{50Ex} < 1$ . Discriminant tsunami potential  $T_{dur} T_d$  and  $T_d T_{50Ex}$  critical threshold for the 25 October 2010 event,  $T_{dur} T_d > 550 \text{ s}^2$  and  $T_d T_{50Ex} > 10 \text{ s}^2$  (tsunami), it remains to rapidly assess  $T_{dur}$  for an earthquake, in particular if  $T_{dur} > 55 \text{ s}$ ,  $T_d > 10 \text{ s}$  and  $T_{50Ex} > 1$ . By using the direct procedure (Lomax and Michelini, 2009; Madlazim, 2011b; Madlazim, 2012), we determined if  $T_{dur}$  for an earthquake is likely to exceed 55 – 60 seconds through HF analysis of vertical-component, broadband seismograms. On 5 – 20 Hz band pass filtered seismogram for local seismograms and on 1 – 5 Hz for teleseismic seismograms (Lomax and Michelini, 2011; Madlazim, 2011b). We formed the ratio of the rms amplitude from 50–60 seconds after the  $P$  with the rms amplitude for the first 25 s after the  $P$  to obtain a station for 50–55 seconds (Lomax and Michelini, 2011; Lomax and Michelini, 2012, Madlazim, 2012). Based on this study and our previous work (Madrilazim, 2011b; Madlazim, 2012), with large earthquakes data sets, we estimate that measures from 11–22 stations are needed to obtain stable estimates of  $T_{dur}$ ,  $T_d$  and  $T_{50Ex}$ .

We identified the most critical parameters for discrimination of earthquake tsunami potential. The performance of the  $T_{dur}$ ,  $T_d$ ,  $T_{50Ex}$ ,  $T_{dur} T_d$  and  $T_d T_{50Ex}$  discriminants, though improved by the  $T_{dur}$ ,  $T_d$ ,  $T_{50Ex}$  values, is dominated by the  $T_d$ ,  $T_{50Ex}$  values (Table 2),  $T_{dur}$  and  $T_{50Ex}$  for large earthquakes is probably related primarily to rupture length,  $L$  and  $T_d$  for large earthquakes is probably related primarily to rupture width,  $W$  and slip,  $D$ . We have shown that  $T_{dur}$ ,  $T_d$ ,  $T_{50Ex}$ ,  $T_{dur} T_d$  and  $T_d T_{50Ex}$  may inherently account for source depth, and that  $T_{dur} T_d$  and  $T_d T_{50Ex}$  may be proportional to Amplitude of the seismogram. These results imply that rupture length,  $L$  and depth,  $z$ , alone can constrain well the tsunami potential of an earthquake. Then information on the fault width  $W$ , and slip  $D$  is of secondary importance, though perhaps provided by  $T_d$  for some event types, or implicitly through scaling relations such as  $W \propto L$  and  $D \propto L$ . There is the suggestion that tsunami potential is more affected by  $T_{dur}$ ,  $T_d$ ,  $T_{50Ex}$ ,  $T_{dur} T_d$  and  $T_d T_{50Ex}$  as function  $LWD$  than the location, depth and  $M_w$  discriminants. The  $T_{dur}$ ,  $T_d$ ,  $T_{50Ex}$ ,  $T_{dur} T_d$  and  $T_d T_{50Ex}$  discriminants were identified better than  $M_w$  and  $T_{dur}$  for these events.

## 6. CONCLUSIONS

The above described analysis based on the inherent sensitivity of  $T_{dur}$  and  $T_{50Ex}$  to rupture length,  $L$  and source depth  $z$ , indicate that the tsunami potential for these earthquake types can be well constrained by the rupture length  $L$  and some mean rupture depth  $z$ . Furthermore, the explicit information on  $T_d$  indicates that the tsunami potential for such earthquake types can be well constrained by the rupture fault width  $W$ , or the mean slip  $D$ , which are parameters of lesser importance.

The results of the analysis imply that the tsunami potential of an earthquake is not a simple function of the potency of  $LWD$  as it is assumed with the use of the  $M_w$  discriminant. To evaluate the

tsunami potential for oceanic reverse earthquakes, further research is needed in finding direct measures and discriminants for events which are occasionally highly tsunamigenic. For the two earthquakes that were analyzed by this study, the  $T_{dur}$ , the  $T_d$ , the T50Ex, the  $T_{dur}$  the  $T_d$  and the  $T_d$ T50Ex discriminants were identified as being better than  $M_w$  and  $T_{dur}$ .

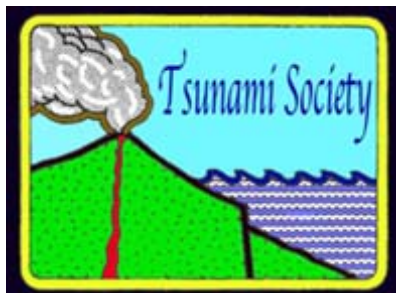
## ACKNOWLEDGMENTS

The GEOFON-BMKG-IA network (<http://webdc.eu>) provided access to waveforms used in this research; I thank all the people who install, operate and maintain the seismic stations in Indonesia. The Global CMT Catalog (<http://www.globalcmt.org/MTsearch.html>) provided access to CMT data used in this research. Furthermore, I thank Anthony Lomax and Michelini who gave us guidance in understanding the rupture duration, dominant period and T50Ex estimation and in applying the SeisGram2k software to estimate these parameters (<http://alomax.free.fr/software.html>). Our discussions with them were beneficial. Finally, I thank Dr. George Pararas-Carayannis for editing certain sections to make them clearer for reading.

## REFERENCES

- Geist, E.L. & Bilek, S.L., 2001. Effect of depth-dependent shear modulus on tsunami generation along subduction zones, *Geophys. Res. Lett.*, 28, 1315–1318, doi:10.1029/2000GL012385.
- Gomez, J.M., Madariaga, R., Walpersdorf, A., and Chalard, E., 2000. The 1996 Earthquakes in Sulawesi, Indonesia, *Bull. Seism. Soc. Am.*, 90, 3, pp. 739–751.
- Hara, T., 2007. Measurement of the duration of high-frequency energy radiation and its application to determination of the magnitudes of large shallow earthquakes, *Earth Planets Space*, 59, 227–231.
- Hirshorn, B. & Weinstein, S., 2009. Rapid estimates of earthquake source parameters for tsunami warning, in *Encyclopedia of Complexity and Systems Science*, p. 10370, ed. Meyers, A., Springer, New York, doi:10.1007/978-0-387-30440-3\_160.
- Kanamori, H., 1972. Mechanism of tsunami earthquakes, *Phys. Earth planet. Int.*, 6, 246–259.
- Lay, T. & S. Bilek, 2007. Anomalous earthquake ruptures at shallow depths on subduction zone megathrusts, in *The Seismogenic Zone of Subduction Thrust Faults*, pp. 692, eds Dixon, T.H. and Moore, C., Columbia Univ. Press, New York, ISBN: 978–0-231–13866-6.
- Lees, 2012, GEOMap: Topographic and Geologic Mapping, <http://cran.r-project.org/web/packages/GEOMap/index.html>
- Lomax, A. & Michelini, A., 2009. Tsunami early warning using earthquake rupture duration, *Geophys. Res. Lett.*, 36, L09306, doi:10.1029/2009GL037223.
- Lomax, A. and A. Michelini, 2011. Tsunami early warning using earthquake rupture duration and P-wave dominant period: the importance of length and depth of faulting, *Geophys. J. Int.* 185, 283–291, doi: 10.1111/j.1365-246X.2010.04916.x.

- Lomax, A. and A. Michelini (2012), Tsunami early warning within 5 minutes, *Pure and Applied Geophysics*, 169, nnn-xxx, doi: [10.1007/s00024-012-0512-6](https://doi.org/10.1007/s00024-012-0512-6)
- Madlazim, Bagus Jaya Santosa, Jonathan M. Lees and Widya Utama, 2010. Earthquake Source Parameters at Sumatran Fault Zone: Identification of the Activated Fault Plane, *Cent. Eur. J. Geosci.*,2(4),2010.DOI:10.2478/v10085-010-0016-5.
- Madlazim, 2011a. CMT, Fault Plane and Rupture Duration for Earthquakes in Sumatra and Possibility of its Implementation for Tsunami Early Warning System, PhD Program of Technology Sepuluh Nopember Institute (ITS) Surabaya. Dissertation.
- Madlazim (2011b), Toward Indonesian Tsunami Early Warning System by Using Rapid Rupture Duration Calculation, *Science of Tsunami Hazards*, Vol 30, No. 4, Tsunami Society International, USA.
- Madlazim (2011c), Menuju Sistem Peringatan Dini Tsunami Menggunakan Perhitungan Durasi Rupture Gempabumi secara Cepat dan Tepat, Edisi 3, 2011, Himpunan Ahli Geofisika Indonesia (HAGI).
- Madlazim, (2011d), Estimasi Durasi, Arah dan Panjang Rupture, serta Lokasi-lokasi Gemabumi Susulan Menggunakan Perhitungan Cepat, *Jurnal Penelitian Fisika dan Aplikasinya (JPFA)*, Vol 2, No. 2.
- Madlazim (2012), Toward tsunami early warning system in Indonesia by using rapid rupture durations estimation, *AIP Conf. Proc.* 1454, pp. 142-145; doi:<http://dx.doi.org/10.1063/1.4730707> (4 pages) INTERNATIONAL CONFERENCE ON PHYSICS AND ITS APPLICATIONS: (ICPAP 2011).
- Madlazim (2012), Menuju Peringatan Dini Tsunami Menggunakan Perhitungan Cepat Periode Dominan dan T50 Exceeds, Seminar Ilmiah Bulanan BMKG "Scientific Journal Club" Kerjasama BMKG-ITS, Surabaya, Kamis, 27 September 2012.
- Nakamura, Y., 1988. On the urgent earthquake detection and alarm system (UrEDAS), in *Proc. of the 9th World Conference on Earthquake Engineering*, Tokyo-Kyoto, Japan.
- Okal, E.A., 1988. Seismic parameters controlling far-field tsunami amplitudes: a review, *Nat. Hazards*, 1, 67–96.
- Polet, J. & Kanamori, H., 2009. Tsunami Earthquakes, in *Encyclopedia of Complexity and Systems Science*, p. 10370, ed. Meyers, A., Springer, New York, doi:10.1007/978-0-387-30440-3\_567.
- Satake, K., 1994. Mechanism of the 1992 Nicaragua tsunami earthquake, *Geophys. Res. Lett.*, **21**(23), 2519–2522.
- Satake, K., 2002. Tsunamis, in *International Handbook of Earthquake and Engineering Seismology*, pp. 437–451, eds Lee, W.H.K., Kanamori, H., Jennings, P.C. & Kisslinger, C., Academic Press, Amsterdam.
- Shearer, P. M. and P. S. Earle, The global short-period wave-field modeled with a Monte Carlo seismic phonon method, *Geophys. J. Int.*, **158**, 1103–1117, 2004.



## SCIENCE OF TSUNAMI HAZARDS

Journal of Tsunami Society International

Volume 32

Number 1

2013

### USING FOURIER TRANSFORM INFRARED (FTIR) TO CHARACTERIZE TSUNAMI DEPOSITS IN NEAR-SHORE AND COASTAL WATERS OF THAILAND

S. Pongpiachan<sup>1\*</sup>, K. Thumanu<sup>2</sup>, W. Na Phatthalung<sup>2</sup>, D. Tipmanee<sup>3,4</sup>, P. Kanchai<sup>1</sup>, P. Feldens<sup>5</sup> and K. Schwarzer<sup>6</sup>

<sup>1</sup>NIDA Center for Research & Development of Disaster Prevention & Management, School of Social and Environmental Development, National Institute of Development Administration (NIDA), Bangkok, THAILAND

\*Corresponding author: [pongpiajun@gmail.com](mailto:pongpiajun@gmail.com)

<sup>2</sup>Synchrotron Light Research Institute (Public Organization), Ministry of Science and Technology, THAILAND

<sup>3</sup>International Postgraduate Program in Environmental Management, Graduate School, Chulalongkorn University, Bangkok, THAILAND

<sup>4</sup>Center of Excellence for Environmental and Hazardous Waste Management (EHWM), Chulalongkorn University, Bangkok, THAILAND

<sup>5</sup>GEOMAR Helmholtz Centre for Ocean Research Kiel, GERMANY

<sup>6</sup>Institute of Geosciences Sedimentology, Coastal and Continental Shelf Research, Christian Albrechts University of Kiel, Kiel, GERMANY

#### ABSTRACT

Understanding the tsunami cycle requires a simple method for identification of tsunami backwash deposits. This study investigates Fourier transform infrared (FTIR) spectroscopy followed by careful analysis of variance (ANOVA), Gaussian distribution, hierarchical cluster analysis (HCA) and principal component analysis (PCA) for the discrimination of typical marine sediments and tsunami backwash deposits. In order to test the suitability of FTIR spectra as innovative methods for classifications of tsunami deposits, typical marine sediments and terrestrial soils were classified into three zones, namely zone-1 (i.e. typical marine sediments), zone-2 (i.e. including tsunami backwash deposits) and zone-3 (i.e. coastal terrestrial soils). HCA was performed to group the spectra according to their spectral similarity in a dendrogram and successfully separate FTIR spectra of all three sampling zones into two main clusters with five sub-clusters. The *simplicifolious* (i.e. single-leaved) type of dendrogram was observed with the strong dissimilarity of terrestrial components in subcluster-5. Graphical displays of PC1 vs PC2 highlight the prominent features of zone-1, which is explicitly

different from those of zone-2 and zone-3. The acceptable discrimination of typical marine sediments and tsunami backwash deposits, even six years after the tsunami on Boxing Day 2004, dramatically demonstrates the potential of the method for the identification of paleotsunami.

**Keywords:** *Tsunami Deposits, Fourier Transform Infrared Spectroscopy (FTIR), Analysis of Variance, Hierarchical Cluster Analysis, Principal Component Analysis, Andaman Sea*

## 1. INTRODUCTION

The 2004 Indian Ocean earthquake is widely acknowledged by the scientific community as one of the world's greatest natural disasters in modern times. The earthquake-generated tsunami caused more than 225,000 of deaths, and damaged the coastal areas of the Indian Ocean countries. The tsunami studies on modern and ancient onshore sedimentary deposits related to the alteration of geological and sedimentological features received massive attention after the Chile tsunami in 1960. For instance, several tsunami-related studies were conducted in North America (Atwater, 1987; Benson et al., 1997; Clague and Bobrowsky, 1994), Thailand (Choowong et al., 2007, 2008a, 2008b, 2009; Szczuciński et al., 2005, 2006, 2007), Papua New Guinea (Gelfenbaum and Jaffe, 2003), Kamchatka (Pinegina and Bourgeois, 2001), Scotland (Dawson et al., 1988; Dawson et al., 1991) and Norway (Bondevik et al., 1997). In addition, the frequency of hurricane/Indian Ocean monsoon (IOM) contributes to the continental input significantly to the offshore regions (Narayana et al., 2008; Scheffers et al., 2009). Despite of a fairly large number of papers dealing with several impacts of the extreme event onshore, little is known about the geomorphological, sedimentological and geological alterations offshore. Since the offshore physical data is substantially crucial for the study of both the modern and past extreme event, it is therefore important to distinguish the difference between terrestrial deposit and background submarine sediment.

In principle, there are several physical evidences to prove the existence of extreme event--originated terrestrial deposits. For example, it is well known that the enrichment of plant debris in sediment can be considered as signatures of terrestrial records (Cantalamesa and Di Celma, 2005; Narayana et al., 2008; Scheffers et al., 2009). However, there are also several problems associated with the employment of these conventional proxies due to its low preservation potential in the submarine environment. Firstly as the plant fragments settle through the water column, several biogeochemical transformations such as remineralization, chemical decomposition and microbial degradation take place. Secondly, the power of wind-generated waves, hurricane/monsoon waves, daily tides, and even anthropogenic activities such as the clean-up of the contaminated sediments coupled with natural bioturbation can dramatically alter both the topographical and sedimentological features of tsunami deposit. Thirdly, there is no single feature to categorize tsunami, hurricane, monsoon and other types of extreme event deposits except through the careful comprehensive investigation of variability in sediment grain-size, shape, roundness, packing, sorting with the precise assessment of the lateral geometry of the entire sedimentary body (Cantalamesa and Di Celma, 2005; Dawson et al., 1988; Dawson and Shi, 2000). In the light of these difficulties, more alternative well-preserved terrestrial indicators are essentially required to enhance the reliability of data interpretation.

In this study, the authors hypothesize that the employment of Fourier Transform Infrared Spectroscopy (FTIR) coupled with various analogies of statistical analysis assist in a better understanding of offshore terrestrial deposit distribution pattern, which can be subject to erosion by tsunami/monsoon waves and surface runoff by heavy rain in the tsunami-affected coastal areas of Andaman Sea, Thailand. Note that it is the purpose of this paper to illustrate the general principle of using organic functional group analyzed by FTIR for the first time as an innovative proxy to separate the terrestrial deposit from the background sediment in tsunami-affected coastal areas. Neither the source apportionment, nor the analysis of spatial variation of organic functional group in sediments is the main focus of this study. In addition, the risks and possibilities of applying FTIR spectral feature as an alternative extreme event proxy will be reviewed and discussed.

## **2. MATERIALS AND METHODS**

### *2.1 Study area and sampling methods*

The Phang Nga coastal zone was chosen as the study area, where is located in the Andaman Sea, eastern part of the Indian Ocean (see Fig. 1). The study area is approximately 1000 km<sup>2</sup> (east-west extension: 25 km, north-south extension: 40 km) where some part was heavily destroyed by the Tsunami 2004. Soil samples were also collected along the coastline from Thub Lamu to Ban Nam Khem in Phang Nga province. The surface sediment samples were collected along the Phang Nga coastal area during December 2007 and March 2010. The criteria for selecting the sampling station was based on the evidence of sedimentary deposit in the study area which Feldens and co-worker (2009) surveyed by using the combination of Multi-beam, Side Scan Sonar and Boomer system. One hundred and seven surface sediment samples were collected by using Van-veen Grab Sampler. Sediment samples were kept in clean aluminum foil, placed in a glass bottle, and stored at - 20°C. After removing stones and shell residuals, they were freeze-dried and sieved to <0.076 mm (200 mesh), and then kept at -20°C until analysis. Soil sampling stations (27 stations) were collected during 18-22 July 2009. The areas, which were affected by the 2004 tsunami (Szcucinski, et al., 2005), were taken into consideration for choosing the sampling station. About a half kilogram of composite sample from 2-m<sup>2</sup> area of each station was collected by using the shovel and then pre-treated as follows as surface sediment samples. All samples were investigated using FTIR to discriminate between the terrestrial sediment and background marine sediment.

### *2.2 FTIR and statistical analysis*

Infrared spectroscopy technique has been widely used for determinations of chemical compositions in sediments (Kovač et al., 2006; Moros et al., 2009; Ramasamy et al., 2009). Recently, in the past few years, FTIR has received much attention as an alternative analytical instrument for determination of organic functional groups in both terrestrial soils and marine sediments because of its relatively fast processing speed, simple operating system and reasonable costs (Moros et al., 2010; Parikh et al., 2008). In this study, the sediment samples were mixed with KBr at various ratios. The optimum

condition for KBr mixing was chosen at 1:15 ratio (sample: KBr) as it gives the highest signal to noise ratio. The mixture was then pressed into a transparent disc in an evacuable pellet die at sufficiently high pressure. The infrared spectra were collected using FTIR Spectroscopy with transmission sampling module and coupled with the highly sensitive mercury cadmium telluride (MCT) detector cooled with liquid nitrogen over the measurement range from 4000 to 600  $\text{cm}^{-1}$ . The measurements were performed with a spectral resolution of 4  $\text{cm}^{-1}$  with 64 scans co-added. (Bruker Optics Ltd, Ettlingen, Germany). The relative integral areas of each peak were then performed using OPUS 6.5 software (Bruker optic, German). In addition, statistical analysis of T-Test, ANOVA, Hierarchical Cluster Analysis (HCA) and Principal Component Analysis (PCA) were performed by using SPSS Version 13.0.

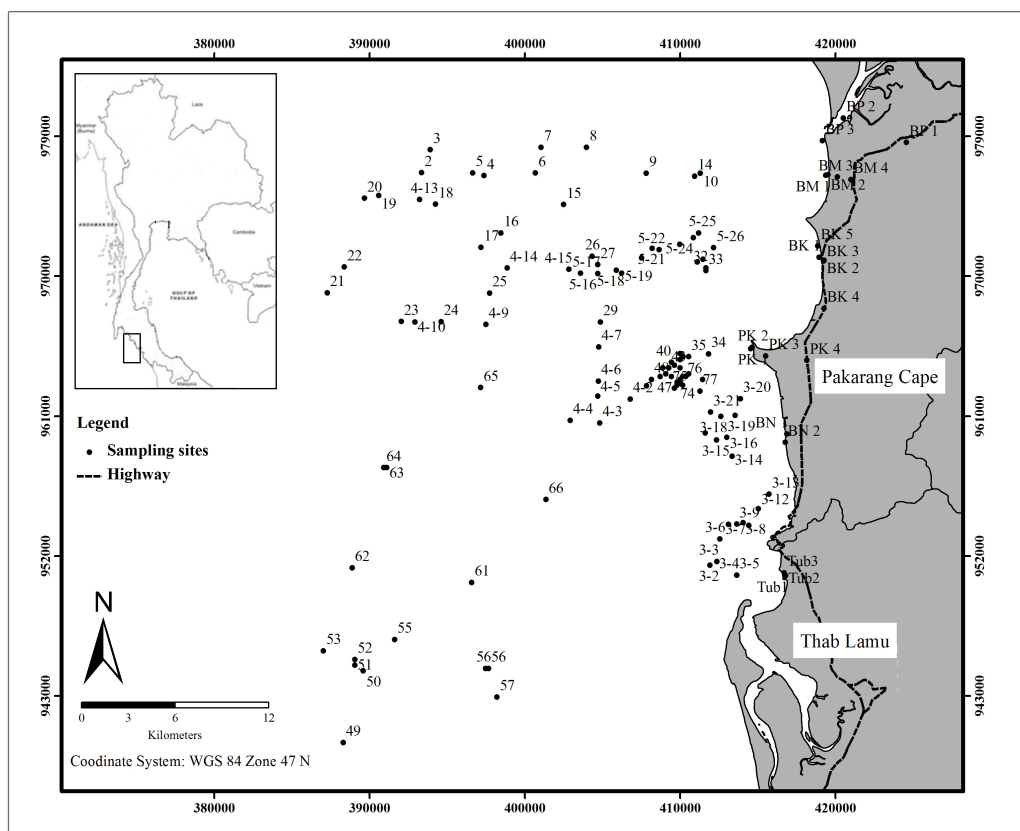


Fig. 1. Sampling site locations at Khao Lak coastal areas, Phang Nga Province, Thailand. (The study area is indicated by the black box; numbers indicate sampling stations).

### 3. RESULTS AND DISCUSSION

#### 3.1. Characteristics of FTIR spectra

In order to test the availability of FTIR spectra as fingerprints for characterization of tsunami deposits, all marine sediments and terrestrial soils were classified into three zones, namely zone-1 (typical marine sediments), zone-2 (tsunami backwash deposits) and zone-3 (coastal terrestrial soils).

All sampling codes and zone descriptions are clearly illustrated in Table 2.

Table 1. Sampling code, date and description of marine sediments and terrestrial soil samples.

Sampling code	Sampling date	Sampling description
		<b>Terrestrial Soil</b>
Tub1	July-18-2009	Canal bank
Tub2	July-18-2009	Tsunami deposit layer
Tub3	July-18-2009	Rubber Plantation
PK 1	July-19-2009	Beach
PK 2	July-19-2009	Tsunami deposit layer
PK 3	July-19-2009	Shrimp pond
PK 4	July-19-2009	Road side
BK 1	July-19-2009	Tsunami deposit layer
BK 2	July-19-2009	Rubber Plantation
BK 3	July-19-2009	Rubber Plantation
BK 4	July-19-2009	Rubber Plantation
BK 5	July-19-2009	Tsunami deposit layer
BN 1	July-20-2009	Canal bank
BN 2	July-20-2009	Canal bank
BM 1	July-20-2009	Tsunami deposit layer
BM 2	July-20-2009	Pond
BM 3	July-20-2009	Rubber Plantation
BM 4	July-20-2009	Palm Plantation
BP 1	July-20-2009	Pond
BP 2	July-20-2009	Mangrove
BP 3	July-20-2009	Nam Khen port
		<b>Sediment</b>
2,3,4,5,6,7,8,9,10	December-1-2007	Pakarang cape sediment
11,12,13,14,15,16,17,18,19,20	December-2-2007	Pakarang cape sediment
21,22,23,24,25,26,27,29	December-3-2007	Tsunami affected sediment
31,32,33,34,35,36,37,39,40,41,42,43,44,45,46,47,48	December-5-2007	Tsunami affected sediment
49,50,51,52,53,55,56,57,58,61,62,63,64,65,66	December-7-2007	Thup Lamu Sediment
68,69,70,71,72,73,74,75,76,77,78	December-8-2007	Tsunami affected sediment
3-1,3-2,3-3,3-4,3-5,3-6,3-7,3-8,3-9,3-10,3-11,3-12,3-13-3-14,3-15,3-16,3-17,3-18,3-19,3-20,3-21,3-23	March-3-2010	Khao lak near shore sediment
4-1,4-2,4-3,4-4,4-5,4-6,4-7,4-9,4-10,4-13,4-14,4-15	March-4-2010	Pakarang cape sediment
5-16,5-17,5-18,5-19,5-20,5-21,5-22,5-23,5-24,5-25,5-26	March-5-2010	Pakarang cape sediment

Table 2. Sample members of each zone

Zone	Sample members	Zone description
Zone-1	25, 04-09, 04-10, 6, 7, 4-13, 16, 17, 18, 19, 20, 22, 50, 52, 53, 55, 56, 49, 57, 61, 62, 63, 64, 66, 23	Zone-1 sediment samples seem not to be affected by tsunami backwash and can be considered as typical marine sediments. All sampling positions were located within the range of 12 to 24 km offshore.
Zone-2	2, 3, 4, 5, 8, 9, 10, 11, 12, 14, 15, 26, 27, 29, 30, 31, 32, 34, 35, 36, 37, 39, 40, 42, 43, 44, 45, 46, 47, 48, 54, 69, 70, 71, 72, 73, 76, 77, 3-02, 3-03, 3-04, 3-05, 3-06, 3-07, 3-08, 3-10, 3-13, 3-14, 3-15, 3-16, 3-17, 3-18, 3-19, 3-20, 3-21, 4-01, 4-02, 4-03, 4-04, 4-05, 4-06, 4-07, 4-08, 4-14, 4-15, 5-12, 5-16, 5-17, 5-18, 5-19, 5-20, 5-21, 5-22, 5-23, 5-24, 5-25, 5-26	According to the acoustic profile data, Zone-2 is most likely to be influenced by the tsunami backwash deposits. All sampling positions were situated within 12 km from the shoreline.
Zone-3	Tub1, Tub2, Tub3, PK1, PK2, PK3, PK4, BK1, BK2, BK3, BK4, BK5, BN1, BN2, BM1, BM2, BM3, BM4, BP1, BP2, BP3	Zone-3 is characterized as natural samples of onshore terrestrial soils.

The FTIR spectra for all sampling zones are compared in Fig. 2. Overall, the spectra of all samples are generally quite similar to each other, which can be characterized by *i*) broad and strong absorption band in the 3750-3000  $\text{cm}^{-1}$  intervals (OH vibration of hydroxyl groups in alumino-silicates and OH vibration of water and OH groups organic fraction of sediments) followed by moderate C-H stretching bands in the interval from 2960 to 2800  $\text{cm}^{-1}$ ; *ii*) moderately strong  $\text{CO}_3^{2-}$  absorption peaks in the frequency range of 2660-2450  $\text{cm}^{-1}$ ; *iii*) the overlap of several possible absorption peaks, namely free water, C-C stretching of aromatics and alkene double bonds, C=O stretch of secondary amides corresponding NH, COO asymmetric stretching of metal carboxylates and carbonate minerals (calcite) in the interval from 1756 to 1268  $\text{cm}^{-1}$  and *iv*) strong Si-O (silicate mineral) absorption peaks in the frequency range of 1270-895  $\text{cm}^{-1}$ .

Although FTIR spectra of all sampling zones display relatively similar distribution pattern in the frequency range from 3750 to 750  $\text{cm}^{-1}$ , some subtle differences were observed in the vibrational modes of organic components indicating the dissimilarities of chemical compositions in each sampling zones. For instance, the prominent feature of three small sharp peaks on the first broad main peak was detected in the interval of 3750-3500  $\text{cm}^{-1}$  of zone-3, highlighting the differences in contribution of hydrogen bond lengths and orientations that mostly corresponding to the OH and NH groups (Wolkers et al., 2004). This can possibly be explained by the relatively high contribution of kaolinite in terrestrial soils, which had previously been mentioned in several studies (Martinez et al., 2010; Rong et al., 2008; Yusiharni and Gilkes, 2012). Interestingly, the characteristic peaks of humic acids (HA) and fulvic acids (FA), which can be explained by two intense bands at 1700  $\text{cm}^{-1}$  and 1640  $\text{cm}^{-1}$  were always observed for all sampling zones. The first absorption band is characterized as C=O stretching vibration of carboxylic acid groups (Mac Carthy and Rice, 1985, Davis et al., 1999 and Richard et al., 2007), whilst the second band is interpreted as the mixture of the stretching vibrations of C=C aromatic bonds, conjugated carbonyl groups (quinone), carboxylic salt groups and amide groups (Vergnoux et al., 2011). Another crucial feature is characteristic peak of lignin spectrum,

which can be assigned to an aromatic  $\nu\text{C}=\text{C}$  stretching vibration in the interval of  $1517\text{--}1509\text{ cm}^{-1}$  (Duarte et al., 2007; Tinoco et al., 2006). Apart from the characteristic peaks of kaolinite, HA, FA and lignin observed in zone-2 and zone-3, the sharp peak appears in the interval range of  $947\text{--}895\text{ cm}^{-1}$  detected in zone-1 emphasizing the influence of relatively high contribution of silicate mineral in typical marine deposits.

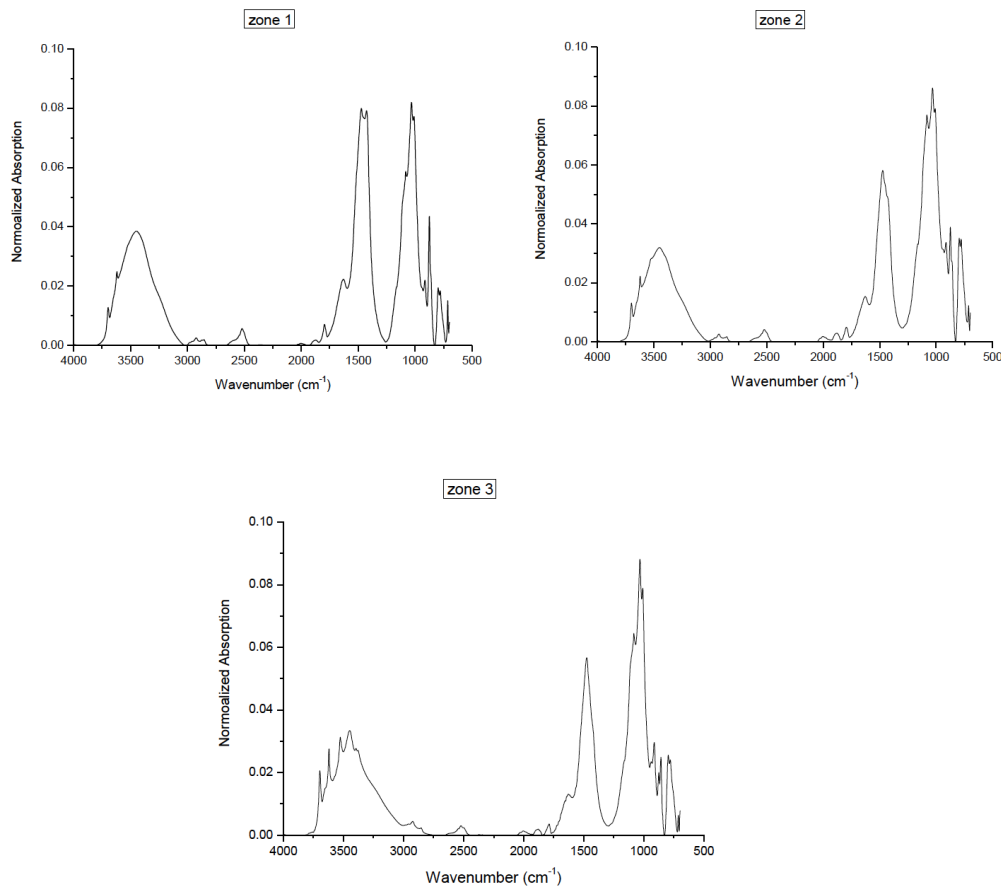


Fig. 2. FTIR spectral of Zone-1, Zone-2 and Zone-3 in  $4000\text{--}500\text{ cm}^{-1}$  frequency range.

### 3.2. Comparison of integrated peak area of FTIR

Averages and standard deviations of integrated peak area of FTIR spectra at 12 different absorption bands (i.e.  $3715\text{--}3608\text{ cm}^{-1}$ ,  $3608\text{--}3048\text{ cm}^{-1}$ ,  $3020\text{--}2800\text{ cm}^{-1}$ ,  $2660\text{--}2450\text{ cm}^{-1}$ ,  $2066\text{--}1930\text{ cm}^{-1}$ ,  $1930\text{--}1846\text{ cm}^{-1}$ ,  $1832\text{--}1760\text{ cm}^{-1}$ ,  $1756\text{--}1600\text{ cm}^{-1}$ ,  $1600\text{--}1268\text{ cm}^{-1}$ ,  $1270\text{--}895\text{ cm}^{-1}$ ,  $895\text{--}831\text{ cm}^{-1}$ ,  $831\text{--}708\text{ cm}^{-1}$ ) of all sampling zones were carefully investigated and compared as shown in Fig. 3. A visual comparison reveals fundamental differences between sampling zones observed in the frequency range of  $3608\text{--}3048\text{ cm}^{-1}$ ,  $1756\text{--}1600\text{ cm}^{-1}$ ,  $1600\text{--}1268\text{ cm}^{-1}$  and  $831\text{--}708\text{ cm}^{-1}$ . Significant differences were observed for these four absorption bands based on the analysis of variance (ANOVA). For instance,

zone-1 shows significantly higher integrated peak area observed in the frequency range of 3608-3048  $\text{cm}^{-1}$  and 1600-1268  $\text{cm}^{-1}$ , which can be explained by relatively larger contribution of OH group organic fractions and calcites as typical chemical components often found in marine sediments (Kovač et al., 2005, 2006). No significant differences of alumino-silicates and carbonate minerals were observed in the interval of 3020-1760  $\text{cm}^{-1}$ , highlighting the homogeneity of these chemical substances in sampling sites. Interestingly, zone-3 displays significantly higher contributions of aromatic compounds and alkene double bond in the absorption bands of 1756-1600  $\text{cm}^{-1}$  that might represent the existence of HA, FA and lignin in terrestrial soils.

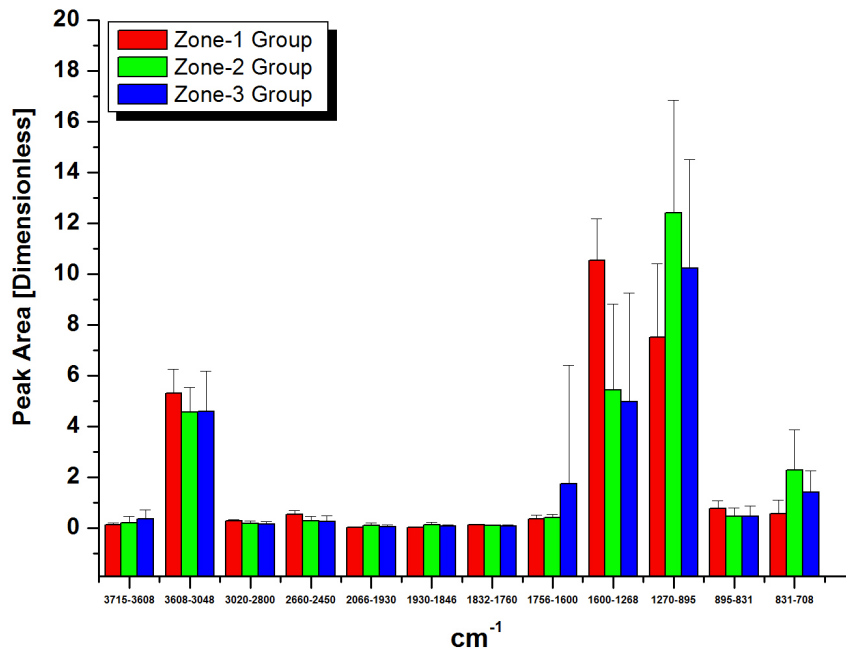


Fig. 3. Integrated peak area of FTIR spectra at 12 different absorption bands for Zone-1, Zone-2 and Zone-3 group.

In order to achieve more comprehensive analysis of FTIR spectra characteristics of each sampling zone, percentage area graphs of 12 absorption bands were plotted and illustrated in Figure 4. Symmetrical triangle shapes of percentage area graphs of all sampling zones appear in the absorption bands from 3715 to 2800  $\text{cm}^{-1}$ . However, the dissimilarity between percentage area graphs becomes apparent at the frequency range of 1756-831  $\text{cm}^{-1}$ . This discrepancy arises essentially from the fact that zone-2 was more influenced by terrestrial materials of zone-3 in comparison with zone-1. Since the FTIR absorption bands from 1756 to 831  $\text{cm}^{-1}$  contain relatively complicated mixture of several organic compounds, mainly HA, FA and lignin, it appears reasonable to interpret the strong similarity of percentage area graphs observed in zone-2 and zone-3 as a consequence of tsunami backwash that

dragged large amounts of terrestrial materials from coastal area into near shore zone.

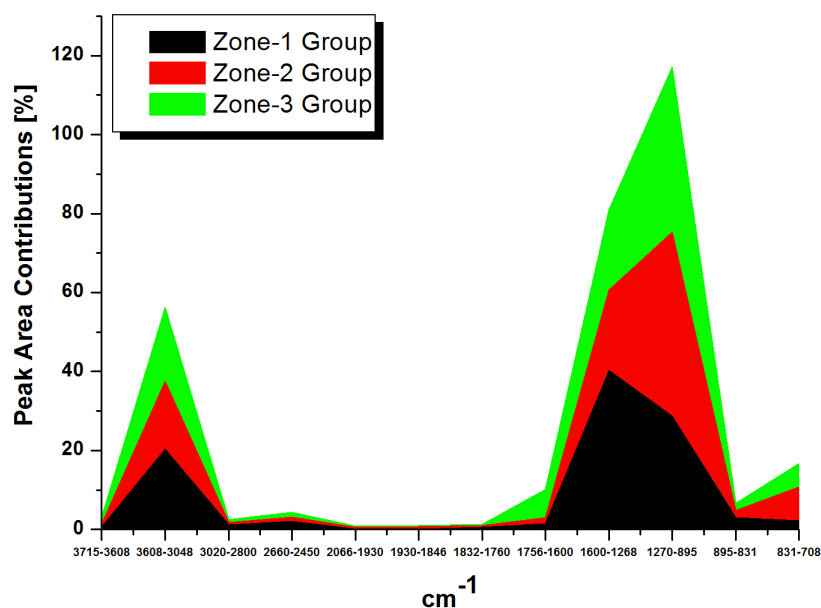


Fig. 4. Percentage contributions of integrated peak areas of FTIR spectra at 12 different absorption bands for Zone-1, Zone-2 and Zone-3 group.

### 3.3 Probability distribution function (PDF)

The probability distribution function (PDF) was applied to all FTIR spectra at 12 different absorption bands as previously mentioned in section 3.2. PDF is a function that explains the comparative probability for this random variable to take on a given value. The probability for the random variable to fall within a particular region is given by the Gaussian distribution, which can be described as follows:

$$y = \frac{1}{\sigma\sqrt{2\pi}} \exp\left(\frac{-(x - \mu)^2}{2\sigma^2}\right) \quad (1)$$

where  $y$ ,  $\sigma$ ,  $\sigma^2$ ,  $\mu$  and  $x$  represent for probability distribution function, standard deviation, variance, average and peak area of spectrum of each zone respectively. As clearly illustrated in Fig. 5, some characteristic features can be extracted directed from the original images. Firstly, a sharp symmetrical bell-shape curve was observed in zone-1 samples for most absorption bands. Since the measured values of the variable are more concentrated in the middle than in the tails, it appears reasonable to assume this fact is a circumstance of moderately homogeneous spatial distribution of organic functional groups in background marine sediments that were much less affected by the tsunami.

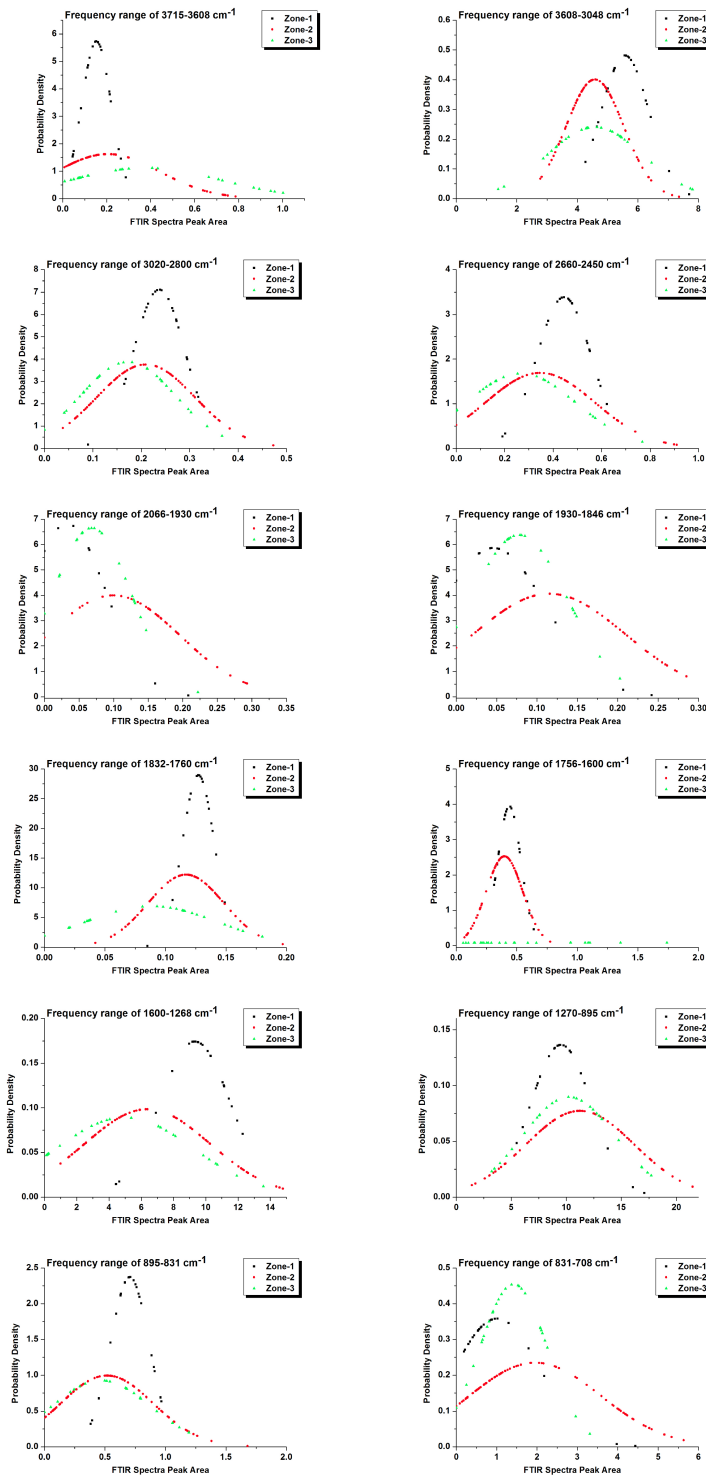


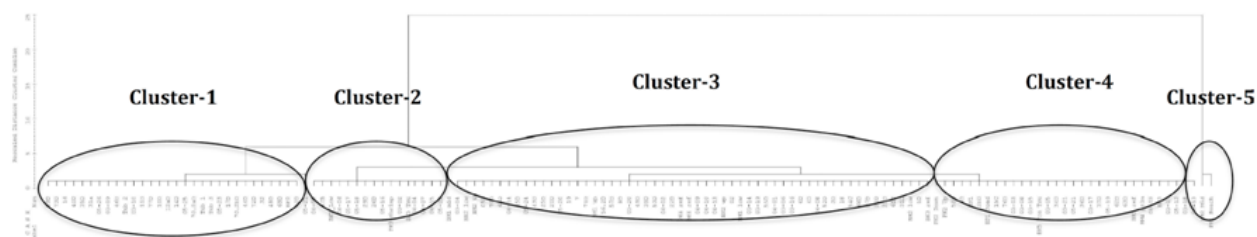
Fig. 5. Probability distribution function graphs of FTIR spectra at 12 different absorption bands of sediment and soil samples collected at zone-1, zone-2 and zone-3.

backwash. For instance, the subtle differences between zone-1 and other zones were detected at the frequency range of 3715-3608  $\text{cm}^{-1}$ , 3020-2800  $\text{cm}^{-1}$ , 2660-2450  $\text{cm}^{-1}$ , 1832-1760  $\text{cm}^{-1}$  and 895-831  $\text{cm}^{-1}$ . This can be inferred as a result of fairly harmonized spatial distribution of kaolinites, CH-stretching mode compounds, carbonates and silicates observed in marine sediments. Secondly, zone-3 shows extremely broad peaks with flat tops at the interval range of 3715-3608  $\text{cm}^{-1}$ , 1832-1760  $\text{cm}^{-1}$  and 1756-1600  $\text{cm}^{-1}$ , emphasizing the high degree of chemical diversity of kaolinite mineral silicates, carbonate minerals, aromatics and alkene double bond components in terrestrial soils. Thirdly, zone-2 demonstrates positive skews in the frequency range of 3715-3608  $\text{cm}^{-1}$ , 2660-2450  $\text{cm}^{-1}$ , 2066-1930  $\text{cm}^{-1}$  and 1930-1846  $\text{cm}^{-1}$ , 895-831  $\text{cm}^{-1}$  and 831-708  $\text{cm}^{-1}$ , indicating that the bulk of spectra peak areas lie to the left of the mean. These asymmetrical distribution curves also reveal the fact that the mean is generally higher than the median and thus underlining the importance of tsunami backwash that dragged large amount of terrestrial materials out to zone-2.

### 3.4 Hierarchical cluster analysis (HCA)

*Hierarchical clustering* allows users to select a definition of distance, then select a linking method of forming clusters, then determine how many clusters best suit the data. *Hierarchical clustering* methods do not require present knowledge of the number of groups. There are three general approaches to clustering FTIR spectra, namely “*Hierarchical Cluster Analysis*”, “*K-means Cluster Analysis*” and “*Two-Step Cluster Analysis*”. In both *K-means clustering* and *two-step clustering*, researchers have to specify the number of clusters in advance, and then calculate how to assign cases to the *K* clusters. Furthermore, these two clustering techniques require a very large scale of data set (e.g.  $n > 1,000$ ). On the contrary, *Hierarchical Cluster Analysis* (HCA) is appropriate for smaller samples (e.g.  $n < 200$ ) and can be carried out without any data pre-treatment (Dach *et al.*, 1999). Therefore, classification of FTIR spectra according to spectral similarity was conducted with the assistance of hierarchical cluster analysis (Fig. 6).

To test the hypothesis that zone-2 contains more tsunami backwash deposits in comparison with those of zone-1, HCA had been conducted on the 12 variables (i.e. 12 different absorption bands as previously mentioned in section 3.2). The HCA revealed the presence of two main clusters with five different sub-clusters. The first major cluster consists of all zone samples with the average percentage contribution of 24%, 56% and 20% for zone-1, zone-2 and zone-3 respectively. This cluster can be divided into four subgroups; the first consists of zone-1 (0%), zone-2 (87%), zone-3 (13%), and the second is composed of zone-1 (47%), zone-2 (29%), zone-3 (24%), the third contains zone-1 (41%), zone-2 (43%), zone-3 (16%) and the fourth constructs zone-1 (10%), zone-2 (64%), zone-3 (26%). According to dendrogram, the members present in the first subgroup can be considered to be a mixture of “tsunami-backwash deposits” and “terrestrial components” with the percentage contribution of 22% ( $n = 30$ ) to all samples ( $n = 136$ ). Cluster-5 is another key-feature in dendrogram, which illustrates the strong presence of terrestrial components namely PK1 and BM2. Since these two samples represent the terrestrial components, it appears reasonable to assume the disagreement of cluster-5 in comparison with other sub-clusters is a consequence of relatively high contribution of HA, FA and lignin.



<b>Cluster-1 (n = 30; Percentage contribution 22%)</b>										
9	73	16	40	35	31	5-26	3-09	46	Tub 2	3-10
11	77	10	13	14	5-25	78	Tub 1	Tub 3	5-23	17
68	44	72	32	48	69	BP2	42			
<b>Cluster-2 (n = 17; Percentage contribution 13%)</b>										
5-21	4-05	47	BK1 low	4-06	5-17	29	26	05-16	PK3	3-02
BK5 Tsu	4-04	4-07	4-15	5-22	BM1 mid					
<b>Cluster-3 (n = 56; Percentage contribution 41%)</b>										
3-04	BN2 low	BM2 up	5	70	64	4-14	45	5-24	43	25
20	5-20	19	7	71	BM1 up	58	57	8	3-20	49
39	53	4-02	22	PK4	BK4	4-09	4-10	4-13	BN2 up	2
BM1 low	3-14	3-19	55	4-01	3-06	3-16	6	42	4-08	52
3	18	54	66	27	30	23	61	41	BM2 low	5
BK3										
<b>Cluster-4 (n = 31; Percentage contribution 23%)</b>										
PK2 down	PK2up	50	4	BN1	33	BP1	15	76	3-03	3-08
3-15	BK5 pre Tsu	3-05	34	3-21	5-21	36	3-17	37	5-19	62
63	BM3	BM4	4-03	BP3	3-07	5-12	3-18	3-13		
<b>Cluster-5 (n = 2; Percentage contribution 1%)</b>										
BM2 mid	PK1									

Fig. 6. Hierarchical cluster analysis of FTIR spectra of terrestrial soils and coastal sediments in the 2004 tsunami-affected Khao Lak area.

### 3.5 Principal component analysis (PCA)

Factor analysis offers the advantages of not requiring prior knowledge of the chemical composition and size distribution of emissions from specific sources (source profiles) but has the drawback of being mathematically indeterminate, allowing a wide range of possible solutions even when it is applied to relatively simple simulated data sets. In natural soils and sediments, which are composed by many potential and diverse sources, principal component analysis (PCA) has been chosen by many researchers for source apportionment of chemical contaminants such as polycyclic aromatic hydrocarbons (Liu et al., 2009; Yunker et al., 2011; Zhang et al., 2012). This technique has also been widely applied to FTIR spectra as main purposes for classifications of biological and chemical materials (Bombalska et al., 2011; Cotrim et al., 1999). In this study, Varimax rotation was selected to maximize the sum of the variances of the squared loadings and thus enable us to seek the similarity of chemical components in sediment and soil samples. FTIR spectra of the samples listed in Table 1 were analyzed by PCA. The principal component patterns for Varimax rotated components of 136 samples composed of three PC, which account for 91.75 %, 6.69 % and 1.47 % for the total of variances of PC1, PC2 and PC3 respectively. The contribution of PC1 and PC2 explains 98.44 % of total variance, and moreover PC1 is 13.7 and 62.4 times higher than PC2 and PC3 respectively.

A plot of the scores of the first two PCs is presented in Fig. 7. It can be easily seen that the full black squares (zone-1) constitute a very broad group along the positive values of PC2 (y-axis) adjacent to 1.0 and then gently decrease exponentially to positive side of PC1 (x-axis). On the contrary, the full black triangle (zone-2) and full black circle (zone-3) resemble each other with a quarter circle curve from north to east, indicating that these samples might share similar organic functional groups. Three possibilities can be considered to be responsible for this phenomenon; *i*) the tsunami inundation might uplift bottom marine sediments to onshore area, *ii*) the tsunami backwash conveyed terrestrial components to marine environment and *iii*) both tsunami inundation and backwash account for the similarity of two-dimensional plots of PCA appearing in Fig. 7. Another key feature is horizontally deviated samples namely 31, 3-9, 5-21, 5-25, 5-26, 10, 14, 42, BK3, BM3, BP2, Tub3 and PK2, which are located parallel to *x*-axis. Since these samples are representative of onshore soils and coastal sediments adjacent to shoreline, it appears reasonable to conclude that the application of PCA on FTIR spectra can successfully discriminate typical marine sediments from terrestrial components and tsunami backwash deposits in near shore and coastal waters of Thailand.

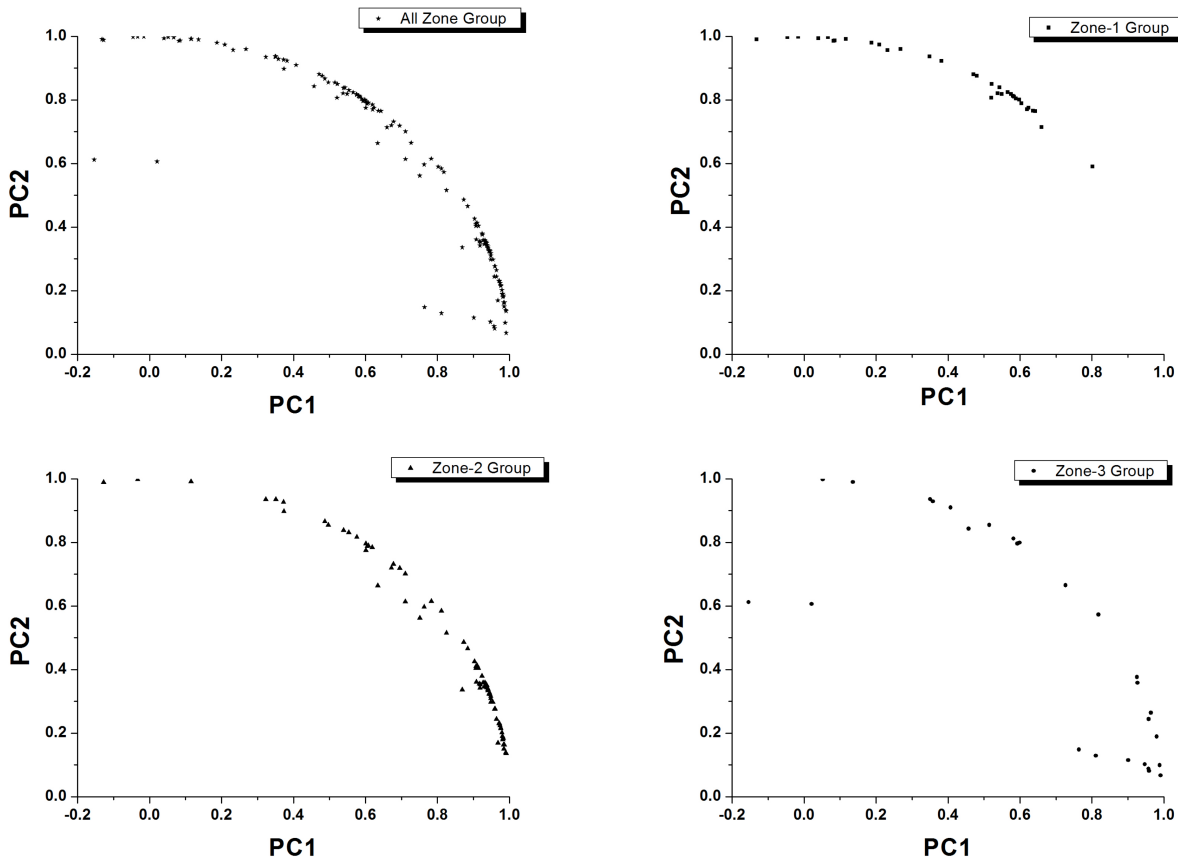


Fig. 7. Two-dimensional plots of PC1 and PC2 using FTIR spectra of terrestrial soils and coastal sediments in the 2004 tsunami-affected Khao Lak area.

### 3.6 Implications for the identification of tsunami deposits

HCA, PDF and PCA analysis of FTIR spectra are able to discriminate terrestrial material in the marine environment. Offshore Khao Lak, tsunami deposits are preserved within fine-grained sediments that were found to be transported towards offshore during normal conditions during the monsoon without the influence of strong events (Feldens et al., 2012). The proxies discussed in this study are thus not able to differentiate between different processes transporting material from on-towards offshore. Nevertheless, they show great potential for the recognition of (paleo) tsunami events: Depending on the local setting, the identification monsoon-generated deposits is possible (e.g., Kempf et al., 2003, Hanebuth and Stattegger, 2004, Schettler et al., 2006) thus allowing to differentiate tsunami and from sediment deposited under normal conditions. In contrast, one of the most discussed concerns in tsunami research is the differentiation between storm and tsunami deposits (e.g., Phantuwongraj and Choowong, 2011, Chagué-Goff et al., 2011, Switzer et al., 2009, Kortekaas and Dawson, 2007, Nott, 2003), especially offshore. No reliable criteria have been developed so far, with rip-up clasts and antidunes being the most characteristic sedimentological differentiation between tsunami and storm deposits in Thailand (Phantuwongraj and Choowong, 2011). However, in general, storms tend to erode the beach and the coastline, and thus transport less material from onshore towards offshore compared to tsunami waves that inundate the hinterland. Thus, when event-layers of uncertain origin are encountered, frequently partly reworked due to erosion or bioturbation, the determination of the terrestrial input within the layer can be a decisive factor for their interpretation. This is especially true for paleotsunamis for which no historical information is available, as the organic functional groups are expected to be preserved within the sediment for at least 12,500 years (Silliman et al., 1996).

Table 3. IR absorptions for representative functional groups

Functional Group & Molecular Motion	Wave number (cm <sup>-1</sup> )*,**
OH vibration of hydroxyl groups in alumino-silicates (Kaolinite mineral silicates)	3715-3608
OH vibration of water and OH groups organic fraction of sediments	3608-3048
CH stretching mode	3020-2800
Carbonate (CO <sub>3</sub> <sup>2-</sup> ) sediment	2660-2450
	2066-1930
Carbonate (CO <sub>3</sub> <sup>2-</sup> ) minerals	1930-1846
	1832-1760
Free water, C-C Stretching of aromatics and alkene double bonds, C=O Stretch of secondary amides corresponding NH, COO asymmetric stretching of metal carboxylates	1756-1600
Carbonate minerals (calcite)	1600-1268
Silicate mineral (Si-O)	1270-951
	947-895
Other carbonates (Li <sup>+</sup> , K <sup>+</sup> , Na <sup>+</sup> )/Other silicate (Overlapping bands)	895-831
	831-708

\*Ramasamy et al., 2009

\*\*Kotoky et al., 2006

#### 4. CONCLUSIONS

The current study showed the high potential of FTIR spectroscopy coupled with hierarchical cluster analysis (HCA) and principal component analysis (PCA) for the discrimination of tsunami backwash deposits and typical marine sediments. According to our best knowledge, this has been the first time that the appropriateness of FTIR spectroscopy for classification of tsunami backwash deposits has been demonstrated. The dissimilarities between the FTIR spectra of all sampling zones were particularly noticeable in the OH vibration of water and OH group organic fraction associated absorption bands from 3608 to 3048  $\text{cm}^{-1}$ , C-C stretching of aromatics and alkene double bonds related frequency range of 1756-1600  $\text{cm}^{-1}$ , calcite linked interval of 1600-1268  $\text{cm}^{-1}$  and other carbonates ( $\text{Li}^+$ ,  $\text{K}^+$ ,  $\text{Na}^+$ ) and silicates at the absorption bands from 831 to 708  $\text{cm}^{-1}$ . Some considerable discrimination of terrestrial components and tsunami backwash deposits was possible with the assistance of HCA, although the separation in some sub-clusters still remain ambiguous and thus reveals a high degree of similarity in FTIR spectra and chemical composition of natural samples in tsunami-affected area. Two-dimensional plots of PCA highlight the similarities of a quarter circle curve from north to east detected in zone-2 and zone-3, which can be explained by the relatively strong influence of terrestrial components dragged by tsunami backwash within 12 km from the shoreline.

#### ACKNOWLEDGEMENTS

This work was performed with the approval of Deutsche Forschungsgemeinschaft (DFG) and National Research Council of Thailand (NRCT). The authors acknowledges all research staff at Phuket Marine Biological Center (PMBC) for their support with ship time of RV Chakratong Tongyai and RV Boonlert Pasook as well as other contributions on other facilities during field measurements. The authors would also like to express special gratitude to Synchrotron Light Research Institute (Public Organization), Ministry of Science and Technology, Thailand for their contribution of FTIR measurements.

## REFERENCES

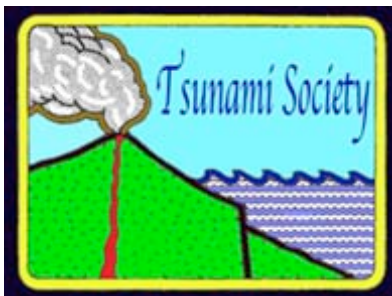
- Atwater, B.F.: Evidence for great Holocene earthquakes along the outer coast of Washington State, *Science.*, 236, 942-944, 1987.
- Benson, B. E., Grimm, K. A., and Clague, J. J.: Tsunami deposits beneath tidal marshes on northwestern Vancouver Island British Columbia, *Quaternary. Res.*, 48, 192-204, 1997.
- Bombalska, A., Oliwa, M. M., Kwaśny, M., Włodarski, M., Kaliszewski, M., Kopczyński, K., Szpakowska, M., and Trafny, A. E.: Classification of the biological material with use of FTIR spectroscopy and statistical analysis. *Spectrochim. Acta. A.*, 78 (4), 1221-1226, 2011.
- Bondevik, S., Sevendsen, J. I., and Mangerud, J.: Tsunami sedimentary facies deposited by the Storegga tsunami in shallow marine basins and coastal lakes, western Norway, *Sedimentology.*, 44, 1115-1131, 1997.
- Cantalamessa, G., and Di Celma, C.: Sedimentary features of tsunami backwash deposits in a shallow marine Miocene setting, Merillones Peninsula, Northern Chile. *Sed. Geol.*, 178 (3-4), 259-273, 2005.
- Clague, J.J., and Bobrowsky, P.T.: Tsunami deposits beneath tidal marshes on Vancouver Island, British Columbia, *Geol. Soc. Am. Bull.*, 106, 1293-1303, 1994.
- Chagué-Goff, C., Schneider, J.L., Goff, J.R., Dominey-Howes, D., and Strotz, L.: Expanding the proxy toolkit to help identify past events—Lessons from the 2004 Indian Ocean Tsunami and the 2009 South Pacific Tsunami, *Earth. Sci. Rev.*, 107, 107–122, 2011.
- Choowong, M., Murakoshi, N., Hisada, K., Charusiri, P., Daorerk, V., Charoentitirat, T., and Chutakositkanon, V., Jankaew, K., and Kanjanapayont, P.: Erosion and deposition by the 2004 Indian Ocean tsunami in Phuket and Phang-nga Provinces, Thailand, *J. Coastal. Res.*, 23(5), 1270–1276, 2007.
- Choowong, M., Murakoshi, N., Hisada, K., Charusiri, P., Charoentitirat, T., Chutakositkanon, V., Jankaew, K., Kanjanapayont, P., and Phantuwoongraj, S.: 2004 Indian Ocean tsunami inflow and outflow at Phuket, Thailand, *Mar. Geol.*, 248(3–4), 179–192, 2008a.
- Choowong, M., Murakoshi, N., Hisada, K., Charoentitirat, T., Charusiri, P., Phantuwoongraj, S., Wongkok, P., Choowong, A., Subsayjun, R., Chutakositkanon, V., Jankaew, K., and Kanjanapayont, P.: Flow conditions of the 2004 Indian Ocean tsunami in Thailand inferred from capping bedforms and sedimentary structures, *Terra. Nova.*, 20, 141–149, 2008b.
- Choowong, M., Phantuwoongraj, S., Charoentitirat, T., Chutakositkanon, V., Yumuang, S., and Charusiri, P.: Beach recovery after 2004 Indian Ocean tsunami from Phang-nga, Thailand, *Geomorphology.*, 104, 134–142, 2009.
- Cotrim, R. A., Ferraz, A., Gonçalves, R. A., Silva, T. F., and Bruns, E. R.: Identifying the origin of lignins and monitoring their structural changes by means of FTIR-PCA and –SIMCA. *Bioresource. Technol.*, 68 (1), 29-34, 1999.
- Dachs, J., Bayona, J. M., Fillaux, J., Saliot, A., and Albaiges, J.: Evaluation of anthropogenic and biogenic inputs into the western Mediterranean using molecular markers. *Mar. Chem.*, 65(3-4), 195-210, 1999.
- Davis, W.M., Erickson, C. L., Johnston, C. T., Delfino, J. J., and Porter, J. E.: Quantitative Fourier transform infrared spectroscopic investigation on humic substance functional group composition, *Chemosphere.*, 38, 2913–2928, 1999.

- Dawson, A.G., Long, D., and Smith, D.E.: The Storegga slides: Evidence from eastern Scotland for a possible tsunami. *Mar. Geol.*, 82, 271-276, 1988.
- Dawson, A.G., Foster, I. D. L., Shi, S., Smith, D.E., and Long, D.: The identification of tsunami deposits in coastal sediment sequences, *Sci. Tsunami. Hazards.*, 9, 73-82, 1991.
- Dawson, A.G., and Shi, S.: Tsunami deposits, *Pur Appl. Geophys.*, 157, 875-897, 2000.
- Duarte, R. M. B. O., Santos, E. B. H., Pio, C. A., and Duarte, A. C.: Comparison of structural features of water-soluble organic matter from atmospheric aerosols with those of aquatic humic substances, *Atmos. Environ.*, 41, 8100-8113, 2007.
- Feldens, P., Schwarzer, K., Szczuciński, W., Stattegger, K., Sakuna, D., and Sompongchaiyikul, P.: Impact of the 2004 Indian Ocean Tsunami on Seafloor Morphology and Sediments Offshore Pakarang Cape, Thailand, *Pol. J. Environ. Stud.*, 18, 63-68, 2009.
- Feldens, P., Schwarzer, K., Sakuna, D., Szczuciński, W., and Sompongchaiyakul, P.: Sediment distribution on the inner continental shelf off Khao Lak (Thailand) after the 2004 Indian Ocean tsunami. *Earth Planets Space.*, 64, 875-887, 2012.
- Gelfenbaum, G., and Jaffe, B.: Erosion and sedimentation from the July 17, 1998 Papua New Guinea tsunami, *Pure. Appl. Geophys.*, 160, 1969-1999, 2003.
- Kortekaas, S., and Dawson, A.G.: Distinguishing tsunami and storm deposits: An example from Martinhal, SW Portugal, *Sediment. Geol.*, 200, 208-221, 2007.
- Kotoky, P., Bezbaruah, D., Baruah, J., Borah, C. G., and Sarma, N. J.: Characterization of clay minerals in the Brahmaputra river sediments, Assam, India, *Curr. Sci.*, 91 (9), 1247-1250, 2006.
- Kovač, N., Faganeli, J., Bajt, O., Orel, B., and Vuk, Š. A.: Investigation of sediment samples from the Gulf of Trieste (northern Adriatic) by FTIR spectroscopy, *Mater. Geoenvi.*, 52(1), 81-85, 2005.
- Kovač, N., Faganeli, J., Bajt, O., Šket, B., Vuk, Š. A., Orel, B., and Mozetič, P.: Degradation and Preservation of Organic Matter in Marine Macroaggregates, *Acta. Chim. Slov.*, 53, 81-87, 2006.
- Liu, Y., Chen, L., Huang, H. Q., Li, Y. W., Tang, J. T., and Zhao, F. J.: Source apportionment of polycyclic aromatic hydrocarbons (PAHs) in surface sediments of the Huangpu River, Shanghai, China. *Sci. Total. Environ.*, 407(8), 2931-2938, 2009.
- Mac Carthy, P., and Rice, J.A.: Spectroscopic methods (other than NMR) for determining functionality in humic substances. In: Aiken, G. R., McKnight, D. M., Wershaw, R. L., MacCarthy, P. (Eds.), *Humic Substances in Soil, Sediment and Water.* John Wiley and Sons, NewYork, pp.527-559, 1985.
- Martinez, E. R., Sharma, P., and Kappler, A.: Surface binding site analysis of Ca<sup>2+</sup>-homoionized clay-humic acid complexes. *J. Colloid. Interf. Sci.*, 352(2), 526-534, 2010.
- Moros, J., Vallejuelo, F. S., Gredilla, A., Diego, D. A., Madariaga, M. J., Garrigues, S., and Guardia, M.: Use of Reflectance Infrared Spectroscopy for Monitoring the Metal Content of the Estuarine Sediments of the Nerbioi-Ibaizabal River (Metropolitan Bilbao, Bay of Biscay, Basque Country), *Environ. Sci. Technol.*, 43, 9314-9320, 2009.
- Moros, J., Cassella, J. R., Alonso, B. C. M., Piñeiro, M. A., Hermelo, H. P., Barrera, B. P., Garrigues, S., and Guardia, M.: Estuarine sediment quality assessment by Fourier-transform infrared spectroscopy. *Vib. Spectrosc.*, 53 (2), 204-213, 2010.
- Narayana, A. C., Jago, C. F., Manojkumar, P. and Tatavarti, R., Nearshore sediment characteristics and formation of mudbanks along the Kerala coast, southwest India.: *Estuarine. Coastal. Shelf. Sci.*, 78, 341-352, 2008.

- Nott, J.: Tsunami or Storm Waves? - Determining the Origin of a Spectacular Field of Wave Emplaced Boulders Using Numerical Storm Surge and Wave Models and Hydrodynamic Transport Equations, *J. Coastal. Res.*, 19, 348–356, 2003.
- Parikh, J. S., Lafferty, J. B., and Sparks, L. D.: An ATR-FTIR spectroscopic approach for measuring rapid kinetics at the mineral/water interface, *J. Colloid. Interface. Sci.*, 320 (1), 177-185, 2008.
- Phantuwongraj, S., and Choowong, M.: Tsunamis versus storm deposits from Thailand, *Nat. Hazards.*, 63, 31–50, 2011.
- Pinegina, T.K., and Bourgeois, J.: Historical and paleo-tsunami deposits on Kamchatka, Russia: long-term chronologies and long-distance correlations, *Nat. Hazard. Earth. Sys. Sci.*, 1, 177-185, 2001.
- Ramasamy, V., Rajkumar, P., and Ponnusamy, V.: Depth wise analysis of recently excavated Vellar river sediments through FTIR and XRD studies, *Indian. J. Phys.*, 83 (9), 1295-1308, 2009.
- Richard, C., Guyot, G., Rivaton, A., Trubetskaya, O., Trubetskoj, O., Cavani, L., and Ciavatta, C.: Spectroscopic approach for elucidation of structural peculiarities of Andisol soil humic acid fractionated by SEC-PAGE setup, *Geoderma.*, 142, 210–216, 2007.
- Rong, X., Huang, Q., He, X., Chen, H., Cai, P., and Liang, W.: Interaction of *Pseudomonas putida* with kaolinite and montmorillonite: A combination study by equilibrium adsorption, ITC, SEM and FTIR. *Colloids. Surf. B.*, 64(1), 49-55, 2008.
- Scheffers, S.R.; Havisser, J.; Browne, T.; Scheffers, A. Tsunamis, hurricanes, the demise of coral reefs and shifts in prehistoric human populations in the Caribbean. *Quatern. Int.*, 195, 69-87, 2009.
- Silliman, E. J., Meyers, A. P., and Bourbonniere, A. R.: Record of postglacial organic matter delivery and burial in sediments of Lake Ontario, *Org. Geochem.*, 24 (4), 463-472, 1996.
- Switzer, A.D., Pucillo, K., Haredy, R.A., Jones, B.G., and Bryant, E.A.: Sea level, storm, or tsunami: enigmatic sand sheet deposits in a sheltered coastal embayment from southeastern New South Wales, Australia, *J. Coastal. Res.*, 21, 655–663, 2009.
- Szczuciński, W., Niedzielski, P., Rachlewicz, G., Sobczyński, T., Ziola, A., Kowalski, A., Lorenc, S., and Siepak, J.: Contamination of tsunami sediments in a coastal zone inundated by the 26 December 2004 tsunami in Thailand, *Environ. Geol.*, 49 (2), 321-331, 2005.
- Szczuciński, W., Chaimanee, N., Niedzielski, P., Rachlewicz, G., Saisuttichai, D., Tepsuwan, T., Lorenc, S., and Siepak, J.: Environmental and geological impacts of the 26 December 2004 tsunami in coastal zone of Thailand—overview of short and long-term effects, *Pol. J. Environ. Stud.*, 15 (5), 793–810, 2006.
- Szczuciński, W., Niedzielski, P., Kozak, L., Frankowski, M., Ziola, A., and Lorenc, S.: Effects of rainy season on mobilization of contaminants from tsunami deposits left in a coastal zone of Thailand by the 26 December 2004 tsunami, *Environ. Geol.*, 53 (2), 253-264, 2007.
- Tinoco, P., Almendros, G., Sanz, J., Gonzalez-Vasquez, R., and Gonzalez-Vila, F.J.: Molecular descriptors of the effect of fire on soils under pine forest in two continental Mediterranean soils, *Org. Geochem.*, 37, 1995–2018, 2006.
- Vergnoux, A., Guiliano, M., Di Rocco, R., Domeizel, M., Théraulaz, F., and Doumenq, P.: Quantitative and mid-infrared changes of humic substances from burned soils. *Environ. Res.*, 111(2), 205-214, 2011.
- Wolkers, W.F., Oliver, A.E., Tablin, F., and Crowe, J. H.: A Fourier-transform infrared spectroscopy study of sugar glasses, *Carbohydr. Res.*, 339(6), 1077–1085, 2004.

- Yunker, B. M., Macdonald, W. R., Snowdon, R. L., and Fowler, R. B.: Alkane and PAH biomarkers as tracers of terrigenous organic carbon in Arctic Ocean sediments. *Org. Geochem.*, 42 (9), 1109-1146, 2011.
- Yusiharni, E., and Gilkes, R.: Rehydration of heated gibbsite, kaolinite and goethite: An assessment of properties and environmental significance, *Appl. Clay. Sci.*, 64, 61-74, 2012.
- Zhang, Y., Guo, S. C., Xu, J., Tian, Z. Y., Shi, L. G., and Feng, C. Y.: Potential source contributions and risk assessment of PAHs in sediments from Taihu Lake, China: Comparison of three receptor models. *Water. Res.*, 46(9), 3065-3073, 2012.

ISSN 8755-6839



**SCIENCE OF TSUNAMI HAZARDS**

---

Journal of Tsunami Society International

**Volume 32**

**Number 1**

**2013**

---

*Copyright © 2013 - TSUNAMI SOCIETY INTERNATIONAL*

*TSUNAMI SOCIETY INTERNATIONAL, 1741 Ala Moana Blvd. #70, Honolulu, HI 96815, USA.*

[WWW.TSUNAMISOCIETY.ORG](http://WWW.TSUNAMISOCIETY.ORG)